UNIVERSIDADE DA BEIRA INTERIOR
Engenharia

Numerical Analysis of a Single Droplet Impinging upon Liquid Films using the VOF Method

Daniel de Almeida Vasconcelos Rodrigues

Dissertação para obtenção do Grau de Mestre em
Engenharia Aeronáutica
(ciclo de estudos integrado)

Orientador: Prof. Doutor André Resende Rodrigues da Silva

Covilhã, outubro de 2018

In memory of my father, Luís Rodrigues

May the chemistry within your heart rest upon your soul

Acknowledgements

First, i would like to express my sincere gratitude to my supervisor, Professor André Resende Rodrigues da Silva, for the valuable support and guidance in writing this dissertation. His motivation and enthusiasm, coupled with immense knowledge, encouraged me to strive towards improving my work.

I am thankful for the opportunity to be affiliated with AeroG - Aeronautics and Astronautics Research Center, directed by Professor Jorge Manuel Martins Barata. This research and development unit provided the resources required for this dissertation.

I am grateful to all my colleagues at AeroG with whom I had the pleasure to devote countless hours to both scientific research and life in general. I would especially like to thank my fellow colleague, PhD student Daniela Ribeiro, for the patience and persistence it took to support me during the ups and downs of researching and writing this dissertation.

I would like to thank my friends who, over these years, shared and experienced memorable moments with me. Not only were we able to support each other but also enriching our academic life and discussing things other than research.

Lastly, I would like to thank my family for their unconditional support and dedication throughout this journey. I personally thank my mother and brother, whose love and guidance were fundamental in my life.

Resumo

Nas últimas décadas, o desenvolvimento de alternativas aos combustíveis fósseis tem-se tornado gradualmente mais relevante. Os biocombustíveis, em particular, atraem interesse, não apenas como uma alternativa ao elevado custo dos combustíveis fósseis, mas também como solução para vários desafios que o mundo moderno enfrenta atualmente. Estes desafios incluem preocupações com a segurança energética, desenvolvimento económico, a necessidade de mitigar a mudança climática e redução das emissões de gases de efeito de estufa.

O principal objetivo desta dissertação é simular numericamente o impacto vertical de uma gota sobre uma superfície líquida com iguais propriedades e envolvida por ar. Foram considerados quatro fluidos: água, 100% Jet A-1 e 75%/25% e 50%/50% de Jet A-1 e NEXBTL, respectivamente. Particularmente, os modelos multifásicos são fenómenos complicados na natureza devido à dificuldade em prever, com precisão, a interface entre as diferentes fases.

O modelo numérico consiste em resolver as equações de Navier-Stokes a partir do método explícito do Volume de Fluido (do inglês, *Volume of Fluid*) para um modelo bidimensional (2D) axissimétrico. Esta análise considera vários parâmetros e métodos para caracterizar a dinâmica do impacto de gotas. As propriedades físicas dos fluidos, a gravidade e os ângulos de contacto são utilizados para clarificar este modelo. Em termos de abordagem dos métodos de solução, o Método de Etapa Fracionária (em inglês, *Fractional Step Method*) resolve numericamente as equações incompressíveis de Navier-Stokes, o esquema de Reconstrução Geométrica (em inglês, *Geometric Reconstruction*) delimita a interface entre o líquido e a gás e o modelo de Força de Superfície Contínua (em inglês, *Continuum Surface Force*) inclui os efeitos da tensão superficial. Os resultados numéricos são validados qualitativa e quantitativamente com os resultados experimentais disponíveis.

Seis cenários diferentes foram simulados numericamente: *Prompt Splash*, *Crown Splash*, *Spreading*, *Jetting*, *Fingering* e *Bubbling*. Os primeiros quatro fenómenos referidos estão de acordo com os resultados experimentais em termos do impacto inicial e da expansão da coroa. O fenómeno de *fingering* apresentou vários problemas relativos ao desenvolvimento da coroa devido à natureza tridimensional (3D) das instabilidades formadas nos limites externos da coroa. O fenómeno de *bubbling* não foi possível de recriar numericamente. É necessário compreender a dinâmica deste fenómeno e como, atualmente, a pesquisa atual é escassa, estudos devem ser feitos para entender as peculiaridades da formação deste tipo de cúpulas. Também foi visualizado a ocorrência de *prompt splash* para as fases iniciais do *crown splash* e do *bubbling*, que não correspondiam aos resultados experimentais. Há várias razões que justificam essa discrepância, como a dificuldade de capturar as gotas extremamente pequenas provenientes da atomização secundária ou os métodos de solução forçarem o *splash* inicial em alguns casos. Em termos de análises futuras, simulações 3D são necessárias para averiguar o número, tamanho e velocidade das gotas provenientes da atomização secundária. O fenómeno de *bubbling* também requer um estudo mais exaustivo no comportamento da dinâmica do impacto das gotas.

Palavras-chave

Impacto de Gotas, Simulação Numérica, método VOF, Jet Fuel, Biocombustível

Abstract

Over the last few decades, developing alternatives to fossil fuels has become increasingly important. Biofuels, in particular, have attracted interest not only as an alternative to expensive fossil fuels but also by providing a solution to several challenges that the modern world currently faces, which include worries regarding energy security, economic development, the need to mitigate climate change and achieving lower greenhouse gas emissions.

The major objective of this dissertation is numerically simulating the vertical impact of a single droplet upon a liquid surface with the same liquid properties and surrounded by air. Four fluids were taken into account: water, 100% Jet A-1 and 75%/25% and 50%/50% of Jet A-1 and NEXBTL, respectively. Particularly, multiphase flows are complicated phenomena in nature due to the difficulty in accurately predicting the interface between the phases.

The numerical model consists of solving the Navier-Stokes equations by means of the explicit Volume of Fluid (VOF) method for a 2D axisymmetric assumption. This analysis considers several parameters and models that define this phenomenon. The physical properties of the liquid and gas, which are density and viscosity, surface tension, gravity and the contact angles of the different fluids represent our physical model. For the solution approach, the Fractional Step Method (FSM) numerically solves the Navier-Stokes incompressible equations, the Geometric Reconstruction scheme tracks the interface between the liquid and the gas phase and the Continuum Surface Force (CSF) model includes the effects of surface tension. The numerical results are validated both qualitatively and quantitatively with available experimental results.

Six different outcomes were numerically simulated: Prompt Splash, Crown Splash, Spreading, Jetting, Fingering and Bubbling. The numerical results for the initial four outcomes are in good agreement with the experimental results in terms of the initial impact and crown expansion. The fingering phenomenon displayed several issues concerning crown development due to the 3D nature of the instabilities formed at the crown rim. The bubbling phenomenon was not possible to numerically recreate. Information regarding the dynamics of this phenomenon is scarce and more research is required to understand the peculiarities of dome formation. It was also visualized prompt splash for the crown splash and bubbling initial stages, which did not correspond to the experimental results. There are several reasons that justify this discrepancy, such as the difficulty in capturing very tiny ejected droplets or the solution approach forcing prompt splash on some of the cases. Overall, 3D simulations are required for future analysis to accurately predict secondary atomization. Work toward the bubbling phenomenon must also be considered.

Keywords

VOF Method, Droplet Impact, Numerical Simulation, Jet Fuel, Biofuel

Index

List of Figures

List of Tables

Nomenclature

Bo	Bond Number	[$-$]
C	Courant Number	[$-$]
C_{max}	Maximum value of the Courant Number	[$-$]
Ca	Capillary Number	[$-$]
D_0	Droplet Diameter	[mm]
D_{in}	Crown Inner Diameter	[mm]
D_{out}	Crown Outer Diameter	[mm]
F	External Body Forces	[N]
F_{CSF}	Surface Tension Force	[N]
Fr	Froude Number	[$-$]
g	Gravitational Acceleration Constant	[m/s^2]
h	Film Thickness	[mm]
h_1, h_2, h_3	Impact Heights: $h_1 = 0.175; h_2 = 0.5; h_3 = 1$	[m]
h^*	Relative Film Thickness	[$-$]
H	Crown Height	[mm]
H^*	Non-dimensional Crown Height	[$-$]
$H2$	Grid Height	[mm]
I	Unit Tensor	[$-$]
La	Laplace Number	[$-$]
L_a	Lenght Scale of Wall Roughness	[mm]
L_{nd}	Non-Dimensional Lenght Scale of Wall Roughness	[$-$]
$\dot{m}$	Mass Flow Rate	[kg/s]
M	Mach Number	[$-$]
n	Normal Surface at the Curvature	[$-$]
$\hat{n}$	Normal Unit	[$-$]
$\hat{n}_w$	Normal Unit Vector to the Wall	[$-$]
Oh	Ohnesorge Number	[$-$]
p	Static Pressure	[$kg/(m.s^2)$]
p_{gauge}	Static Gauge Pressure	[$kg/(m.s^2)$]
Re	Reynolds Number	[$-$]
R_a	Arithmetical Mean Value of Wall Roughness	[mm]
R_{nd}	Non-Dimensional Arithmetical Mean Value of Wall Roughness	[$-$]
S_m	Source Term	[$-$]
S_{α_q}	Source Term	[$-$]
t	Time	[ms]
Δt	Time Step	[ms]
$\hat{t}_w$	Tangential Unit Vector to the Wall	[$-$]
U	Velocity	[m/s]
U_0	Droplet Impact Velocity	[m/s]
U_{x_i}	Velocity in the x_i direction	[m/s]
$V1$	Grid Radial Distance	[mm]
Δx_i	Length Interval in the x_i direction	[mm]
We	Weber Number	[$-$]

Greek symbols

α	Volume Fraction	[$-$]
κ	Interface Curvature	[$-$]
μ	Dynamic Viscosity	[$mPa.s$]
μ^*	Dynamic Viscosity Ratio	[$-$]
ρ	Density	[kg/m^3]
ρ^*	Density Ratio	[$-$]
σ	Surface Tension	[mN/m]
τ	Non-dimensional Time	[$-$]
$\overline{\overline{\tau}}$	Stress Tensor	[$-$]
θ_w	Static Contact Angle	[$\circ$]

Subscripts

0	Refers to the Droplet
g	Gas phase
l	Liquid Phase
p	p Phase
q	q Phase
w	Wall

Acronyms and Abbreviations

2D	Two-Dimensional
3D	Three-Dimensional
ANSYS	Analysis of Systems
BIM	Boundary Integral Method
CFL	Courant-Friedrichs-Lewy
CICSAM	Compressive Interface Capturing Scheme for Arbitrary Meshes
CLSVOF	Coupled Level Set and Volume of Fluid Method
CPU	Central Processing Unit
CSF	Continuum Surface Force
CSS	Continuum Surface Stress
DNS	Direct Numerical Simulation
FSM	Fractional Step Method
HRIC	High Resolution Interface Capturing
HVO	Hydrotreated Vegetable Oil
ITA	Iterative Time-Advancement
JF	Jet Fuel
LBM	Lattice-Boltzmann Method
LSM	Level Set Methods
MAC	Marker and Cell
MATLAB	Matrix Algorithm
MPS	Moving Particle Semi-Implicit
MUSCL	Monotonic Upwind Scheme for Conservation Laws
NEXBTL	Neste Renewable Diesel
NITA	Non-Iterative Time-Advancement
PISO	Pressure-Implicit with Splitting of Operations
PRESTO!	Pressure Staggering Option
QUICK	Quadratic Upstream Interpolation for Convective Kinematics
SIMPLE	Semi-Implicit Method for Pressure-Linked Equations
SPH	Smooth Particle Hydrodynamics
UBI	Universidade da Beira Interior
VOF	Volume of Fluid

Chapter 1

Introduction

This dissertation focuses on numerically simulating the droplet impact phenomenon onto liquid films. The current chapter presents an initial introduction to this topic.

The first section describes the motivation in biofuels and numerical analysis, the second section enumerates the different objectives for the current work and the third and final section displays the structure of this dissertation.

1.1 Motivation

Over the last few decades, developing alternatives to fossil fuels has become increasingly important. Biofuels, in particular, have attracted interest not only as an alternative to expensive fossil fuels but also by providing a solution to several challenges that the modern world currently faces, which include worries regarding energy security, economic development, the need to mitigate climate change and achieving lower greenhouse gas emissions [1].

The issue regarding energy security relies on the fact that there are few alternatives to fossil fuels when it comes to transportation and fuelling internal combustion engines. Introducing biofuels allows to diversify some of the reliance on fossil energy sources and to manufacture home-produced fuels. Increasing the investment in biofuels also promotes economic development, including the creation of new jobs and sources of income for farmers. This would mostly benefit developing countries, in which a large proportion of the population is employed in agriculture, in the demand for world energy. With the appropriate method of production, biofuels will produce significantly lower greenhouse gas emissions than those emitted by the current fossil fuels. Although most of the current aircraft and heavy vehicles have no carbon-neutral alternative options, the current civil aviation legislation allows for fuel mixtures up to 50% of biofuel, which implies a minimum percentage of 50% of jet fuel.

This dissertation is focused on numerically simulating droplet impact phenomenon onto liquid films. It appears in a wide variety of engineering areas such as ink-jet printers, internal combustion engines, spray cooling, among others. The research of this study has been motivated by the need for a better predictive capability in these industries. Ribeiro [2] experimentally studied this phenomenon using jet fuel and biofuel mixtures and this work will provide a comparison between the experimental and the numerical results.

Numerical analysis relies on solving equations of a certain mathematical model to try and represent a physical phenomenon. Specifically, multiphase flows couple the Navier-stokes equations with an interface-tracking method in order to represent how different phases respond when coexisting in the same environment. These flows are complicated to represent and, since the complex interactions between the droplet and the liquid film are still far from being fully understood, the current methods might not be accurate enough to predict the different interactions between the phases. Therefore, since the use of numerical simulations is becoming progressively

important with the increase in computing power available, improving efficiency and reliability on our simulations is of interest.

1.2 Objectives

A proper understanding of multiphase models and droplet impact dynamics is still lacking, both experimentally and numerically. The main objective of this dissertation is accurately predicting the different outcomes visualized by Ribeiro [2] using the Volume of Fluid (VOF) method. Accomplishing it requires the following:

- Numerical simulation of the six different outcomes visualized by Ribeiro [2];
- Validation and verification of the mathematical model and numerical approach, respectively;
- Comparison between the numerical and the experimental results in terms of crown development, splashing and outcome.

1.3 Overview

This dissertation is organized as follows: Introduction, Literature Review, Numerical Setup, Results and Discussion and Conclusions and Future Work.

The first and current chapter includes the motivation presented for this dissertation, concerning biofuels and numerical methods, the objectives provide an accurate description of the specific actions taken to reach a certain goal and the overview refers to the thesis organization on the different chapters and subjects.

The second chapter is dedicated to the review of the bibliography regarding droplet impact dynamics for both experimental and numerical fields. This includes non-dimensional numbers, classification of impact targets, such as dry and wetted surfaces, droplet dynamics referring to the splashing phenomenon and crown development and, lastly, a variety of numerical methods capable of predicting interactions between different phases.

The third chapter describes the numerical model. Initially, the Volume of Fluid (VOF) model is meticulously explained in terms of its applications, governing equations and specific models. Afterwards, the numerical approach to the physical model is presented, as the geometry, meshing, boundary conditions, adopted models, solution approach and initialization are detailed. A grid independence study is performed to guarantee validation of the numerical results, as well as a comparison between experimental and numerical data.

The fourth chapter exhibits the numerical analysis of the different outcomes and the comparison with the experimental results in terms of splashing, crown evolution and overall development of the phenomena. The final chapter presents the conclusions and possible future work for this dissertation.

Chapter 2

Literature Review

The current chapter unveils the overall phenomenon of the single droplet impact. The first section presents the main factors that influence the droplet impact dynamics on liquid films and the dimensionless parameters that govern this kind of impact. This section is an introduction to the mechanisms of drop impact.

The second section is dedicated to the impact target classification, which includes dry and wetted surfaces. Even though the splash morphology on a dry surface may be similar to that on a liquid film, the mechanisms that lie underneath for the two surface targets are fundamentally different. Therefore, distinct types of impact are presented for these surfaces and a deeper explanation of how the different parameters affect crown development in terms of thickness, height, diameter, etc, is presented.

Recognizing that the splashing and the non-splashing phenomena involve different processes and exhibits such different patterns is the first step in understanding how the droplet behaves when impinging on liquid films. Therefore, the third section fully describes droplet splashing, which results from high energy impact. Every aspect that might determine if splashing occurs or not, such as viscosity, surface tension, etc, is presented. The influence of these parameters on the formation of secondary droplets in terms of size, number and stage are also reviewed.

The fourth and last section of this chapter is dedicated to numerical methods. Different numerical models that have been adopted to simulate droplet impact upon liquid films are reviewed, such as grid-based methods, Lagrangian particle methods, among others. Several differences are stated between them, as the main purpose of this section is introducing the following chapter that is fully dedicated to the VOF method and the numerical analysis of impacting droplets.

2.1 Introduction

The phenomenon regarding impact of single drops onto a liquid film is rather interesting and complex. It has a great number of applications on different fields such as internal combustion engines, spray cooling, pesticide spraying of crops [3], soil and stone erosion [4], atomization of dangerous liquids, dispersal of spores and micro-organisms and coating process, among others. This phenomenon is mostly seen in nature when the raindrops impinge on already wetted surfaces on the ground.

Despite the different applications, scientific research on drop impact is mainly driven by its applications in industrial technology and equipment due to its favourable heat and mass transfer potential and, although the researchers have been studying this content for decades, the complex interactions between the droplet and the liquid film are still far from being fully understood.

The following sections establish the necessary background to understand the droplet impact

phenomenon regarding impact target classification, drop impact mechanisms, the main factors that influence the drop impact dynamics, non-dimensional parameters, etc.

2.2 Non-dimensional Parameters

According to Yarin [5] and Motzkus [6], the main parameters that define the droplet impact on liquid films are divided into three categories: the liquid drop, the liquid film and the surrounding air. The different combinations of these properties define a variety of dimensionless parameters that govern the impact dynamics on liquid films. These parameters involve the Reynolds number, the Weber number, the Ohnesorge number, the Laplace number, the Froude number, the Capillary number, among others. A thorough explanation of the non-dimensional parameters is presented in order to comprehend the mechanisms behind droplet impact.

As reviewed by Yarin [5] and Liang [7], there are several dimensionless parameters involving these phenomena. Some of the most important dimensionless numbers for this kind of impact are the Reynolds number, Re, the Weber number, We, and the Ohnesorge number, Oh. The Reynolds number is defined as the ratio between the inertial and viscous forces, the Weber number relates the inertial to the surface tension forces and the Ohnesorge number is represented as the ratio between the viscous forces and the inertial and the surface tension forces, as seen in equations 2.1, 2.2 and 2.3, respectively:

$$Re = \frac{\rho_l D_0 U_0}{\mu_l} \quad (2.1)$$

$$We = \frac{\rho_l D_0 U_0^2}{\sigma} \quad (2.2)$$

$$Oh = \frac{\mu_l}{\sqrt{\rho_l \sigma D_0}} = \frac{\sqrt{We}}{Re} \quad (2.3)$$

where ρ is the density, D_0 is the droplet diameter, U_0 is the droplet impact velocity, μ is the dynamic viscosity, σ is the surface tension and the subscript l refers to the liquid phase. The Ohnesorge number can also be represented as the ratio between the square root of the Weber number and the Reynolds number.

Following this, there are other three non-dimensional parameters that, despite not being relevant to this dissertation, are worth mentioning. The Froude number, Fr, is defined as the ratio between the inertial and the gravitational forces, the Capillary number, Ca, is described as the ratio between the viscous and the surface tension forces and the Bond number, Bo, represents the ratio between the gravitational and the surface tension forces. Respectively, the parameters are represented by the equations 2.4, 2.5 and 2.6.

$$Fr = \frac{U_0}{\sqrt{g D_0}} \quad (2.4)$$

$$Ca = \frac{\mu U_0}{\sigma} = \frac{We}{Re} \quad (2.5)$$

$$Bo = \frac{\rho_l g D_0^2}{\sigma} = \frac{We}{Fr} \quad (2.6)$$

where g is the gravitational acceleration constant. Since gravity effects can be neglected for $Fr \geq 10$ [5, 8], then gravity effects are not important when considering the phenomenon of droplet impact.

The Laplace number, La, is described by the ratio between the surface tension forces and the momentum-transport (especially dissipation) inside a fluid and it is defined by the equation 2.7. It can also be expressed through non-dimensional parameters.

$$La = \frac{\rho_l \sigma D_0}{\mu_l^2} = \frac{Re^2}{We} \quad (2.7)$$

According to Liang [9], the ratios of liquid-gas density and viscosity are also important to characterize the drop impact on a liquid film. They are represented by equation 2.8 and 2.9, respectively:

$$\rho^* = \frac{\rho_l}{\rho_g} \quad (2.8)$$

$$\mu^* = \frac{\mu_l}{\mu_g} \quad (2.9)$$

where the subscript g refers to the gas phase. The last non-dimensional parameter referred to in this section is the non-dimensional time. It is described as the ratio between the product of the impact velocity and time, t, and the droplet diameter. This non-dimensional parameter characterizes the different stages of the droplet impact phenomenon and is expressed by equation 2.10.

$$\tau = \frac{U_0 t}{D_0} \quad (2.10)$$

Although the different non-dimensional parameters have been presented and thoroughly described, an explanation of how the droplet reacts regarding the impact target is now needed. As mentioned before, the mechanisms that define each type of impact targets are fundamentally different and need to be reviewed.

2.3 Classification of impact targets

In general, impact targets can be classified into dry and wetted surfaces. Over this section, the different mechanisms between dry solid surfaces and liquid films are distinguished. Droplet impact onto liquid films with a dimensionless thickness greater than one will not be considered here, as the condition of droplet impact onto films with dimensionless thickness, smaller than unity, is often satisfied in the engine environment [10]. The dimensionless thickness, as one of the most important non-dimensional numbers for droplet impact onto liquid films, is profoundly explained over subsection 2.3.2. Despite the work of this dissertation being focused on the

numerical simulation of droplet impact on wetted surfaces, a deep understanding of dry solid surfaces and liquid films is necessary to comprehend the differences behind this two impact surfaces.

2.3.1 Dry Surfaces

The phenomena which occur when a single droplet impacts on a non-heated dry surface exhibits different mechanisms that depend on many factors, such as the interface and the impact conditions. Figures 2.1 and 2.2 display several outcomes, differently enumerated, regarding this kind of impact. Those outcomes are basically identified as stick (i), spread (ii) and splash (iii). During spread, it might occur fingering (iv) and, at later stages, the droplet may rebound (v) from the surface. Rioboo et al. [11] added the occurrence of fingering (iv), already mentioned, and replaced the term ”splash” with ”disintegration”. Four disintegration mechanisms were differentiated, which involve prompt splash (iii-a), corona splash (iii-b), receding breakup (iii-c) and partial rebound (iii-d). More recently, Moita and Moreira [12] added a new mechanism, denominated the finger breakup (iii-e). Later on, these different phenomena will be thoroughly interpreted.

According to Bai and Gosman [13] and Rioboo et al. [11], we can distinguish these phenomena by their impact energy and time scale, respectively, as displayed on figures 2.1 and 2.2.

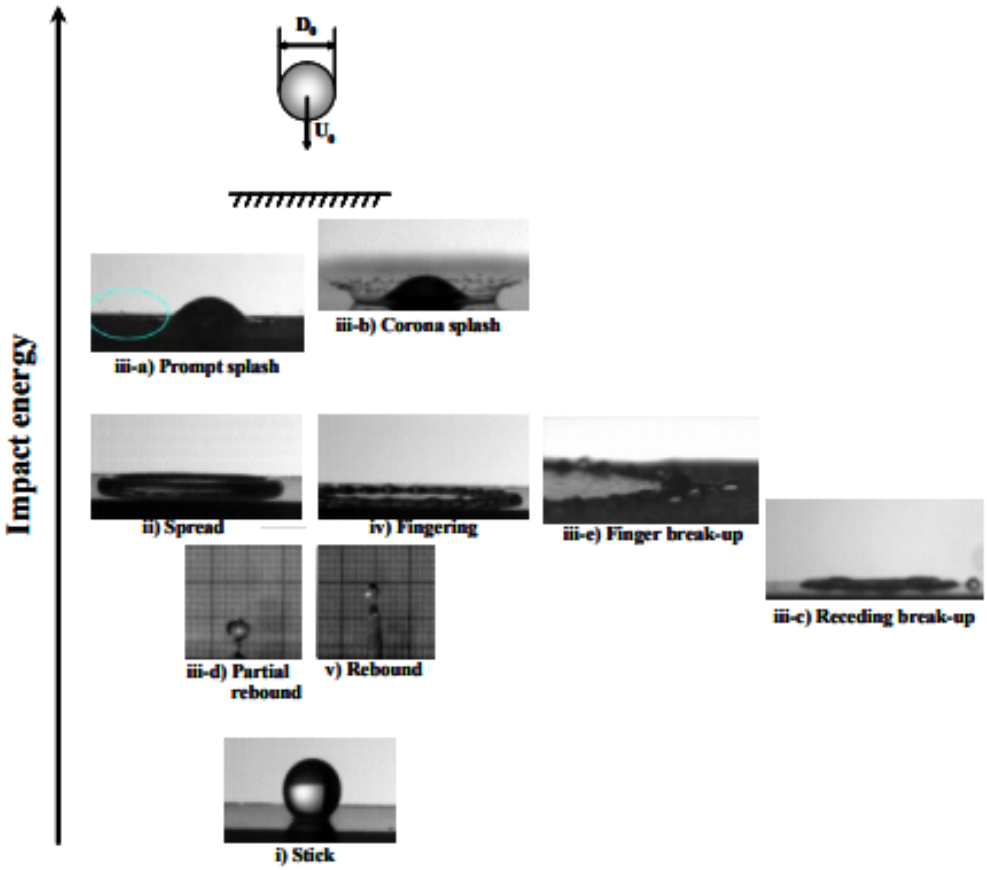

Figure 2.1: Outcome of single droplets impacting onto non-heated dry surfaces based on its impact energy by Bai and Gosman [13].

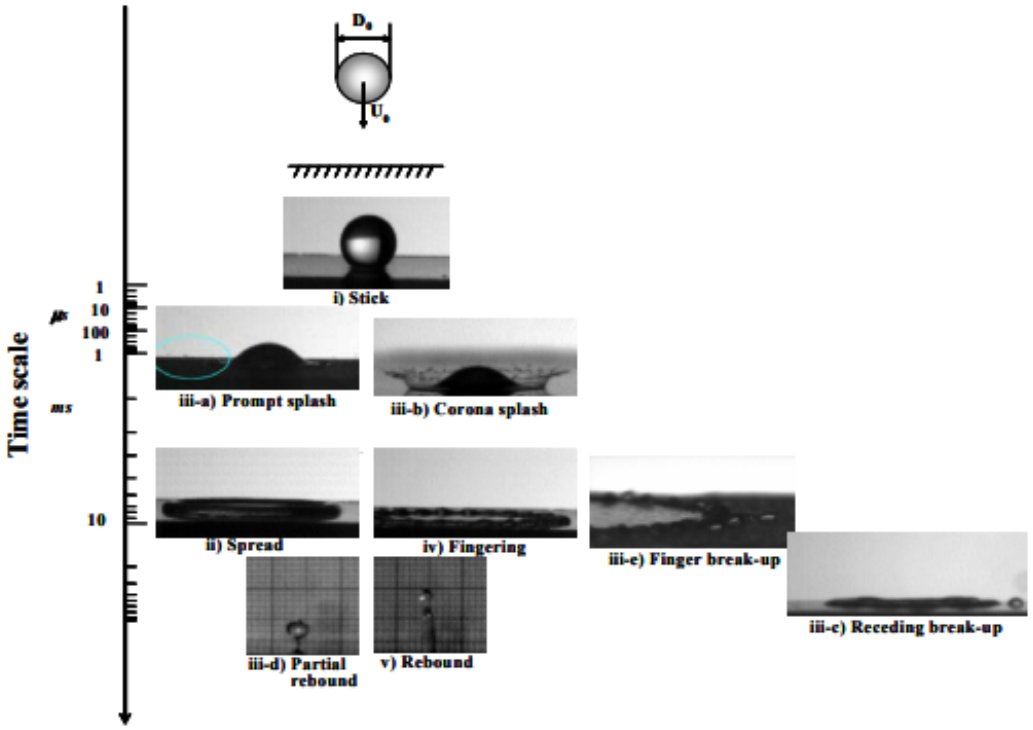

1

Figure 2.2: Outcome of single droplets impacting onto non-heated dry surfaces based on its time scale by Rioboo et al. [11].

At low impact energy values, the droplet sticks to the wall but, as the impact energy increases, a lamella forms which spreads and recoils until all the energy is dissipated. At certain impact velocities, the rim of the lamella may start to destabilize when the spreading phase begins, which may lead to the formation of regular structures called fingers, which grow ahead of the contact line and further breakup during the last stages of spreading, e.g. Yoon and Desjardin [14]. These structures were studied by several authors [15, 16, 17]. However, Yarin [5] reviewed with detail the fundamentals of the fingering mechanism.

In order to better comprehend dry surfaces, since the phenomena also occur with certain similarity on wetted surfaces, a deeper explanation is presented.

2.3.1.1 Stick

This outcome occurs when the impact energy is very low. Once the droplet impacts with the surface, it keeps its spherical shape. This kind of outcome is only seen for impacts on dry surfaces and the droplet tends to maintain its spherical shape, also due to the surface roughness.

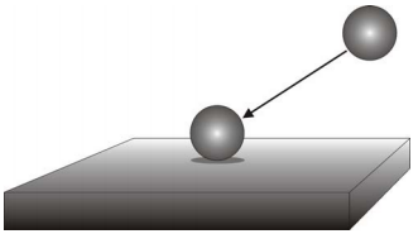

Figure 2.3: Stick regime illustration by Silva [18].

2.3.1.2 Deposition/Spread

According to Rioboo et al. [11], deposition is said to occur when the droplet spreads on the surface at impact and remains attached at the surface during the entire impact process without the formation of secondary droplets. It also occurs for low impact energy values. Bai and Gosman [13] defined the same phenomenon as spread. However, Coppola et al. [19] established some differences between these two phenomena. Despite both representing droplets merging with the liquid surface without emitting any kind of secondary atomization, deposition occurs at lower impact velocities where the impact fails to generate capillary waves. These waves are created when thin liquid sheets emitted subsequent to impact grow into a lamella that propagates radially, thus creating capillary waves. In this dissertation, deposition and spreading are defined as the same phenomenon, following the same terminology as Ribeiro [2].

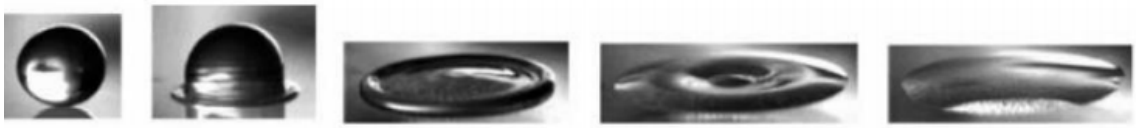

Figure 2.4: Deposition regime illustration by Rioboo et al. [11].

2.3.1.3 Prompt splash

The prompt splash is promoted by a higher impact energy on rough surfaces. Once the droplet impacts the surface, it disintegrates, resulting in tiny droplets detaching from the periphery of the liquid lamella generated by the spreading drop. At the end of this process, the droplet spreads on the wall. This kind of splash occurs at the beginning of the spreading phase.

Figure 2.5: Prompt splash regime by Rioboo et al. [11].

2.3.1.4 Corona splash

The corona splash, also called crown or delayed splash, occurs when the liquid lamella detaches from the wall, forming droplets around the rim of a corona. This phenomenon occurs at a later stage of the impact process and it is also characteristic on liquid film impact.

Figure 2.6: Corona splash regime by Rioboo et al. [11].

2.3.1.5 Receding breakup

As the liquid retracts from its maximum spreading radius, due to the fact that the contact angle decreases during retraction, if the limiting value of zero is reached, it may cause some drops to be left behind by the receding lamella.

Figure 2.7: Receding breakup regime by Rioboo et al. [11].

2.3.1.6 Complete and Partial rebound

Only occurs when a drop recedes after impact, e.g., if a receding phase is observed. According to Ribeiro [2], this phenomenon can also be called jetting and, since the terminology should match between these dissertations, this outcome is defined as jetting in this dissertation as well. As the drop recedes to the impact location, the kinetic energy of the impinging drop causes the liquid to extend vertically through the centre, forming a vertical liquid column called ”jet”. If, due to capillary instability, the droplet can stay partly at the surface and launch one or more droplets at its top, it is denominated partial rebound. However, if it detaches from the surface as an intact drop, it is denominated as complete rebound.

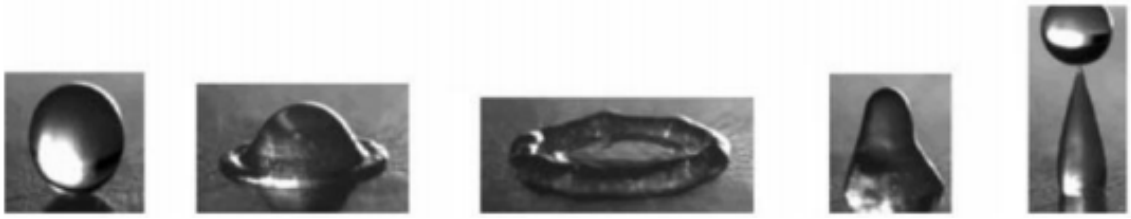

Figure 2.8: Partial rebound regime by Rioboo et al. [11].

Figure 2.9: Complete rebound regime by Rioboo et al. [11].

2.3.1.7 Fingering and Finger Breakup

According to Marmanis and Thoroddsen [16] and Yarin [5], when, during the drop impact, there are certain disturbances that affect the associated patterns of the impact, mostly azimuthal disturbances, their growth results in fingering at the rim of a spreading drop on a dry wall. This phenomenon was also reported by Ribeiro [2] in liquid films with a dimensionless thickness of 0.1. If, however, the developed fingers experience further breakup, likely due to capillary instability, secondary droplets are ejected. This phenomenon is defined as Finger Breakup.

Figure 2.10 displays the fingering and the finger breakup regime and, despite this particular case occurring on a wet surface, this figure was preferred for the visualization of the phenomenon.

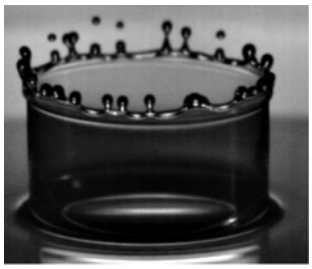

Figure 2.10: Fingering and Finger Breakup regime. Adapted from Deegan et al. [8].

2.3.2 Wetted Surfaces

The impact of single drops on thin liquid films was studied to understand the mechanism of secondary atomization of sprays colliding on a wetted, cold, solid surface. Before starting to address these impact mechanisms, it is important to determine how liquid films are defined. Tropea and Marengo [20] identified and divided liquid films into four different categories.

Table 2.1: Various impact regimes for impact on a wetted surface. Adapted from Tropea and Marengo [20].

Regime	Range	Impact characteristics
Thin liquid film	$L_{nd} < h^* < 3R_{nd}^{0.16}$	Impact depends on surface features
Medium liquid film	$3R_{nd}^{0.16} < h^* < 1.5$	Impact is weakly dependent on surface features
Shallow pool	$1.5 < h^* < 4$	Impact depends on film thickness but is independent of surface characteristics
Deep pool	$h^* > 4$	Impact is independent of film thickness

In order to understand the different ranges for the different regimes, there are some equations that need to be introduced.

Equation 2.11 describes one of the most important non-dimensional numbers used to define liquid films, which is dimensionless thickness. It is described as the ratio between film thickness and drop diameter and different values of this number will result in different outcomes. Equations 2.12 and 2.13 refer to the arithmetical mean value of wall roughness, R_a, and length scale of the wall roughness, L_a, also non-dimensionalized by the drop diameter, respectively.

$$h^* = h/D_0 \quad (2.11)$$

$$R_{nd} = R_a/D_0 \quad (2.12)$$

$$L_{nd} = L_a/D_0 \quad (2.13)$$

Before introducing the different stages of drop impact on liquid films, we have to separate and present the differences between splash and deposition. In this dissertation, and to follow the terminology adopted by Ribeiro [2], the term splash will be used to indicate the formation of secondary droplets after the impact of the impinging drop and the term deposition will indicate an impact without the production of secondary droplets.

Despite most of the phenomena found on dry surface impact being similar to those found on wetted surface impact, as well as most of them occurring on both conditions, there are particular differences that must be mentioned.

Another possible outcome, barely mentioned in the literature, is bubbling. Reported by Macklin and Metaxas [21], this phenomenon consists on the formation of a dome or bubble after a crown splash event. The bubbling episode is essentially defined by liquid films with a higher relative thickness, such as deep pools. However, Ribeiro [2] reported this same phenomenon for a dimensionless thickness of $h^* = 0.5$.

Since droplet impact on wetted surfaces is a rather complex phenomenon and involves a massive number of variables, a profound definition of the different stages of this kind of impact is required.

There are five different stages regarding droplet impact on liquid films. Figure 2.11 represents the initial phase of this phenomenon. The droplet starts its vertical descent from a predefined height, gaining velocity as it approaches the liquid film. We can observe different parameters from the droplet, the gas and the liquid film, as mentioned in section 2.2.

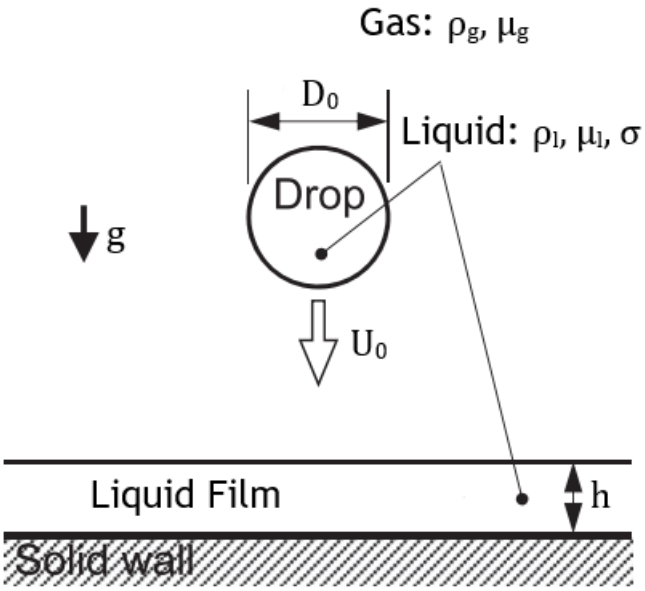

Figure 2.11: Visual representation of a droplet approaching the liquid film. Adapted from Liang [7].

Figure 2.12 represents the formation of the ejecta sheet. Once the droplet impacts the liquid film, a thin axisymmetric sheet arises during the earliest stages of the impact. This particular sheet emerges through the neck region between the droplet and the bottom layer where the two liquid masses connect. According to Thoroddsen [22], the ejecta sheet is originated from the underlying liquid film, not the liquid droplet. Josserand and Zaleski [23] concluded that viscosity plays a major role in the neck region, defining the width of the ejecta sheet that will later develop into a crown. Surface tension serves to either allow or prevent the formation

of the ejecta sheet. If the existing conditions are not favourable, the ejecta sheet will not develop. However, if it develops due to favourable conditions, this sheet becomes the leading edge of the crown sheet and it starts to bend down, colliding with the liquid film and breaking up immediately, causing prompt splash. This occurrence may cause irregularities in the crown sheet and rim. The remaining initial ejecta sheet is pulled up by the developing crown, as observed in figure 2.13.

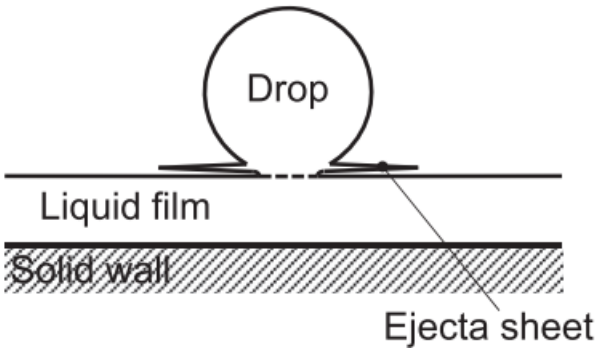

Figure 2.12: Visual representation of the ejecta sheet. Adapted from Liang [7].

Figure 2.13 displays the transition from the initial impact, where the ejecta sheet may be formed, into the initial crown formation. The ejecta sheet keeps its horizontal shape while the crown wall height increases due to the crown development. The liquid film outside of the crown wall, which we denominate as the initial film, remains its initial thickness. However, the liquid film located inside the crown wall (the impact region between the droplet and the film) has its thickness reduced, due to the fact that part of the crown wall liquid derives from the liquid film underneath.

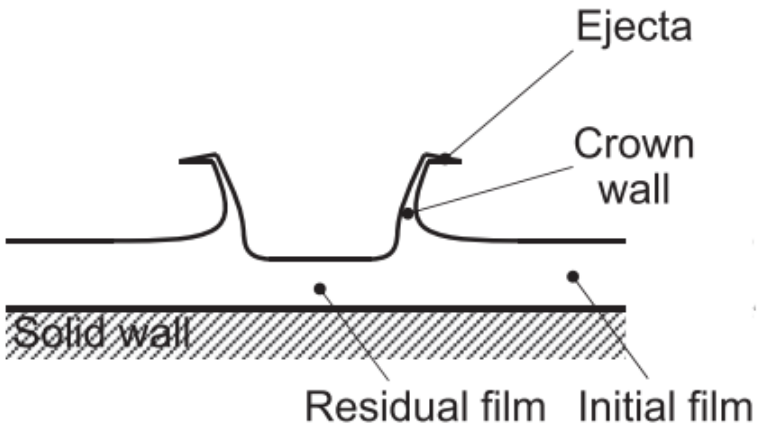

Figure 2.13: Visual representation of the crown evolution by Liang [7].

Once the crown fully develops, there are two possible outcomes. The first outcome is the crown formation without splashing, which means there are no secondary droplets ejected from the rim. The second outcome is the crown formation with splashing, which is represented by figure 2.14. This outcome is characterized by the detachment of the liquid lamella from the crown wall, forming droplets around the rim of a corona, as described in section 2.3.1.4.

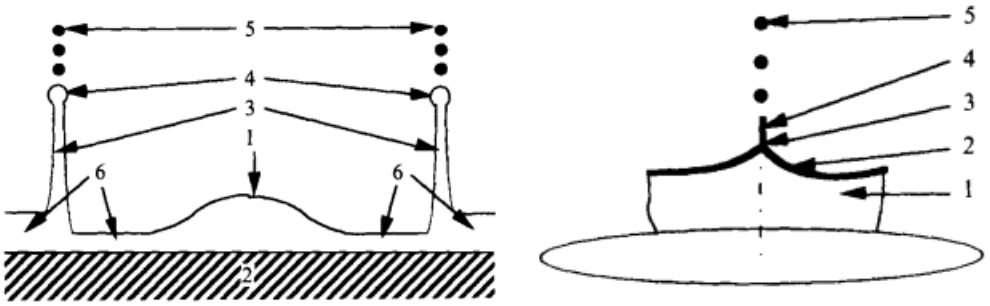

(a) (b)

Figure 2.14: Crown splash representation by Yarin and Weiss [24]: (a) Sketch of splashing mechanism: 1 - residual top of impacting drop; 2 - wall; 3 - section of crown-like sheet propagating outwards; 4 - cross-section of free rim; 5 - secondary droplets formed from cusps of free rim; 6 - liquid layer on wall. (b) Free rim and secondary droplets magnified: 1 - crown-like sheet; 2 - free rim at its top edge; 3 - cusp; 4 - thin jet emerging at cusp; 5 - secondary droplets formed on breakup of jet.

There are different aspects that characterize the crown development itself. There is the crown wall, the free rim, the liquid film inside and outside of the crown, as well as the formation of secondary droplets from the free rim if the conditions are favourable. The occurrence of splashing will be detailed thoroughly in the following section.

The crown evolution may depend on several factors, such as liquid viscosity, dimensionless thickness, etc. These factors may alter the way how the crown evolves, as in faster development, smaller height or even thinner crown walls. The crown formation can be divided into four main geometrical parameters: height, thickness, angle and diameter. Many authors investigated, experimentally and numerically, different parameters and their influence on crown evolution. Despite the current efforts to fully understand the mechanisms behind crown development, there still is inconsistency between different authors.

The crown height, H, is defined as the vertical distance between the crown base and the rim. Non-dimensional crown height, $H^* = H/D_0$, is mentioned by several authors to study crown height evolution. Cossali et al. [25] reported an experimental study on the time evolution of various parameters, namely the crown height. It was disclosed that the evolution of the crown height (the non-dimensional crown height, H^*, and the correspondent non-dimensional time, τ) depend on the Weber number (in particular the impact velocity) but is weakly dependent on the film thickness. Davidson [26] numerically investigated the evolution of the deforming liquid surface subsequent to the impact of a droplet onto a film of the same liquid. Results were that, for a specific time, the crown height increased with increasing film thickness. Mukherjee and Abraham [27] performed an axisymmetric analysis of drop impingement on walls with a pre-existing liquid film. It was concluded that when the dimensionless film thickness is relatively low ($h^* < 0.25$), the rate of increase of the crown height increases with the increase of h^*. However, for higher values of h^* ($h^* > 0.25$), the crown height develops in a differing way, decreasing with the increase of h^*.

The crown diameter is described as the radial extent of the crown. Since the crown is usually non-cylindrical, its diameter is not constant along the crown. Coghe et al. [28] defined two different diameters, which are the crown base diameter and the top rim diameter.

Liang et al. [29] simulated the influence of the Weber number, Reynolds number and non-dimensional film thickness on the crown height and diameter. Regarding crown height, it was

reported that it increases with the increase of the Weber number, while the effect of the dimensionless thickness shows some complexities, as already mentioned. Conclusions about crown diameter showed that it can be increased by decreasing the dimensionless thickness, while the Weber and Reynolds numbers have no effect on it.

Despite several authors [30, 31] complying with Liang [29] results, there are still lots of disagreements regarding the evolution of crown geometrical parameters. As already mentioned, Mukherjee and Abraham [27] concluded that the crown diameter increases with increasing film thickness when the liquid film is thin ($h^* < 0.25$). However, for thicker liquid films ($h^* > 0.25$), the crown diameter tends to decrease with increasing film thickness.

Just like the crown diameter, the crown is not a cylindrical wall of uniform thickness and, therefore, there is no possibility of defining a single thickness throughout the crown. It is possible, however, to estimate the crown thickness as half the difference between the outer and the inner diameter, which can be denominated as normal thickness. This way, it is possible to study the crown thickness evolution and how it interacts with the different parameters.

Experimental work is scarce regarding crown thickness evolution due to the fact that, according to Fujimoto et al. [32], detailed temporal and spatial distributions of crown thickness can only be determined from numerical simulations. It was also concluded that crown thickness decreases with decreasing surface tension.

The crown angle refers to the angle at the base of the crown. This angle is not constant along the crown due to the wall curvature. There are not many reports in the literature specifically regarding the crown angle. Fedorchenko and Wang [33] proposed a dynamic model in order to study the central jet development, which allowed to determine the angle between the crown wall and the liquid film. It was reported that the crown angle is determined entirely by its dimensionless thickness. For $h^* > 0.25$, the crown angle is constant and assumes the value of 90º. For $h^* < 0.25$, the crown angle gradually decreases with h^*.

2.4 Splashing phenomenon

The splashing phenomenon occurs at relatively high droplet impact velocities and it is characterized by the formation of smaller droplets that occur subsequent to the droplet impact. According to Cossali et al. [34], secondary atomization occurs on two different splashing cases: prompt and delayed splash.

Overall, splashing can be influenced by viscosity and surface tension. Motzkus et al. [35] concluded that inertial forces benefit the splashing phenomenon while the viscous forces and surface tension favour the development of deposition. Liang et al. [36] and Cossali et al. [34] experiments were focused on trying to understand the mechanism of secondary atomization, in order to compare the different interactions between the droplet impact and the liquid film in terms of non-dimensional parameters. They concluded that the prompt and delayed splash were highly dependent on the liquid viscosity, which corresponds to the Ohnesorge number. Prompt splash occurs mainly for low Ohnesorge values, while delayed splash is associated with high Ohnesorge values.

Motzkus et al. [37] carried an experimental investigation on the generation of airborne particles during the droplet impact onto a liquid film. This study related the droplet impact velocity,

which is correlated with the Weber number, and the dimensionless thickness with the number and size of the secondary droplets. It was reported that the mass and number of the ejected secondary droplets increased with the increase of the Weber number and with the decrease of the dimensionless thickness. Those secondary droplets are smaller in prompt splash than in delayed splashing, which can be explained by the fact that less energy is required for prompt splash to occur and, consequently, droplets of smaller diameter are ejected.

Vander Wal et al. [38] also concluded that both surface tension and viscosity play a major role on this kind of impact. High surface tension delays the formation of secondary droplets, whether the small droplets are ejected from the spreading of a drop onto a dry surface or from a developing crown upon droplet impact onto a liquid film. In other words, high surface tension inhibits splashing whether the impact target is dry or covered by a thin liquid film. Viscosity, however, does not affect the different impact targets in a similar way. It promotes splashing when the surface is dry and it retards splashing when the surface is covered with liquid film.

The surronding gas and its properties may also influence splashing. Liang et al. [9] numerically investigated the influence of the gas density and viscosity on the crown behaviour and the occurrence of splashing. Numerical results show that gas density and viscosity affect the crown evolution and the splashing mechanism, respectively. Figure 2.15 shows the effect of the density ratio on the crown shape.

We can conclude from figure 2.15 that the gas density has no influence on splashing, however, it affects the crown development. For high density ratio values, the crown develops into higher heights and the crown rim bends outwards. As the density ratio decreases, the crown rim changes shape, as it goes from an outward bending position to a nearly vertical shape. With further decrease of the density ratio, the rim starts to bend inwards. It is apparent that, regardless of the density ratio, there is the occurrence of splashing.

Figure 2.16 presents the effect of the viscosity ratio on the crown behaviour. Decreasing the viscosity ratio shows an inhibition in terms of crown development, as well as suppressing the existence of splashing. This influence can be noted from the early stages of the impact. At $t = 0.1ms$, for viscosity ratios higher than $\mu^* = 0.05$, there is a jet in the contact region of the droplet and the liquid film, as for lower viscosity ratios that jet does not develop. At later stages, the crown develops and splash occurs for high viscosity ratios. However, for lower viscosity ratios, the crown does not fully develop and splashing may be inhibited.

Several other authors [39, 40, 41] demonstrated that splashing on a dry surface can be completely suppressed by decreasing the pressure of the surrounding gas. Therefore, similar gas pressure effects may be expected for droplet impact onto liquid films.

The formation of secondary droplets may occur at different stages of the droplet impact. Deegan et al. [8] showed that there are at least three sources of secondary droplets: small droplets are ejected from the prompt instability of the ejecta sheet, medium-sized droplets are ejected from the rim instability of the ejecta sheet and large droplets are ejected from the rim instability of the crown sheet. Each source refers to a different stage of the phenomenon. The small droplets develop the moment the droplet impinges upon the liquid film, the medium-sized droplets develop on the transition between the ejecta sheet and the crown formation and large droplets develop once the crown is fully developed through the formation of fingers, which break into secondary droplets.

Several authors researched secondary atomization with the purpose to better understand splash-

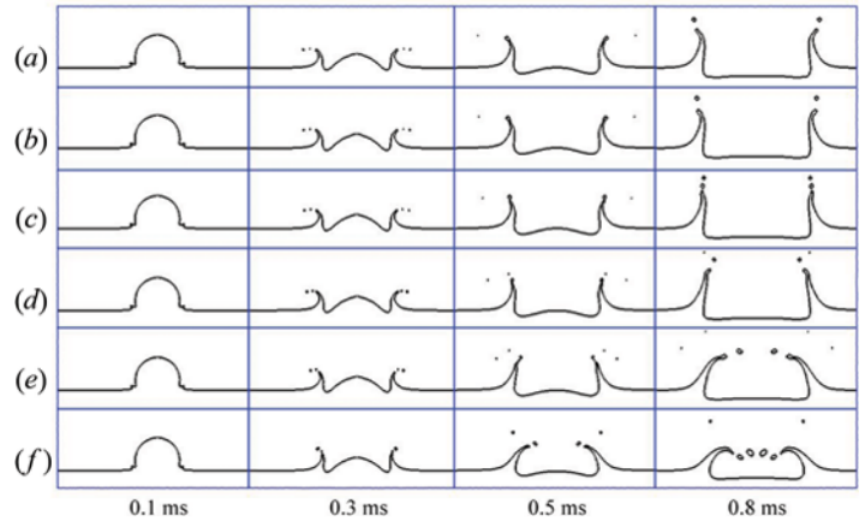

Figure 2.15: The effect of the density ratio on the crown shape: (a) $\rho^* = 815$, (b) $\rho^* = 400$, (c) $\rho^* = 200$, (d) $\rho^* = 100$, (e) $\rho^* = 50$, and (f) $\rho^* = 25$ by Liang et al. [9].

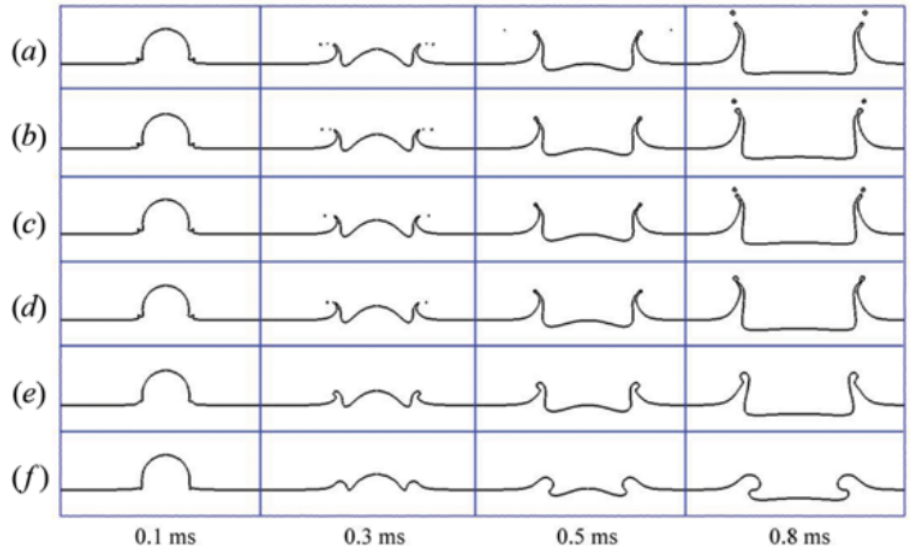

Figure 2.16: The effect of the viscosity ratio on the crown shape: (a) $\mu^* = 56$, (b) $\mu^* = 5$, (c) $\mu^* = 1$, (d) $\mu^* = 0.5$, (e) $\mu^* = 0.05$, and (f) $\mu^* = 0.01$ by Liang et al. [9].

ing and its influences. Cossali et al. [34] studied the splashing employing various mixtures of water and glycerol. It was reported that, for high Ohnesorge numbers (high viscosity), there is a higher number of fingers on the crown than on low Ohnesorge numbers (low viscosity). It was also verified that, for higher Weber numbers, the droplets detaching from the fingers occur at earlier stages with a low non-dimensional diameter while, for lower Weber numbers, that same detaching occurs for earlier and later stages, with the latter presenting higher non-dimensional parameter than the former.

Vander Wal et al. [38] reported that an increase in surface tension or viscosity increases the size and decreases the number of secondary droplets. This was also verified by Davidson [26] and Motzkus et al. [6] regarding surface tension and viscosity, respectively. Motzkus et al. [6] experimental investigation was based on establishing the influence of various parameters regarding the droplet, the liquid film and the surrounding gas onto the formation of secondary atomization. It was concluded that an increase in both impact velocity and diameter of the

droplet increase the size of the secondary droplets emitted on impact. However, the influence of the dimensionless thickness did not display such a linear correlation. Results show that, for an impact velocity of $U_0 = 3.1m/s$, h^* does not affect the number of secondary droplets emitted. However, for an impact velocity of $U_0 = 3.7m/s$, a decrease of h^*, from 0.6 to 0.3, results in an increase in the number of emitted droplets. Other authors, such as Hobbs and Osheroff [42] and Gregory et al. [43] reported that the total number of droplets produced increased as the film thickness decreased. This was verified for thin liquid films with a depth smaller than $h = 1mm$.

2.5 Numerical Methods Applied to Single Droplet Impact

Reliable and accurate modelling of many industrial processes require accounting for interactions between different phases. A large number of flows encountered in nature are defined as multiphase flows, such as conversion of crude to high-value petroleum products in a refinery, combustion of coal to generate energy in a power plant and combustion of gasoline droplets in an internal combustion engine. Particularly, two-phase flow is a complicated phenomenon in nature due to the existence and deformation of the interface between liquid and gas, which are the primary reasons behind two-phase flow simulations.

The reason behind multiphase model development, as well as technological improvement, relies on the fact that, in most cases, practical experiments are costly and time-consuming. Therefore, numerical simulations are of interest for a variety of industrial processes.

The successful design of equipment and processes that involve multiphase flows crucially depends on accurately predicting the interactions between the phases. Since most of these processes are impossible to observe, engineers rely on models and experiments to gain insight into improving efficiency, throughput, safety and reliability. In fact, one of the key challenges in simulating multiphase flows, namely droplet impact, is achieving an accurate interface.

Since the main focus of this dissertation is multiphase models regarding droplet impact onto liquid films, which involves liquid-gas interface, distinct numerical simulations must be presented and explained as an introduction to this topic.

Harlow and Shannon [44] were the first to numerically simulate drop impact onto a liquid film. In order to investigate the splash of a liquid droplet onto dry and wetted surfaces, the full Navier-Stokes equations are solved numerically using the Marker and Cell (MAC) technique. This technique, developed by Harlow and Welch [45], consisted in solving problems in the dynamics of an incompressible fluid with a free surface, which can be applied on several problems, such as the splash of a linear drop, the splash of a falling column of water, among others. Since then, there has been quite a development of numerical methods, in order to try and represent this phenomenon.

The Volume of Fluid (VOF) method has become quite popular in 2D and 3D simulations. Developed by Hirt and Nichols [46], the VOF method can model two or more immiscible fluids by solving a single set of momentum equations and tracking the volume fraction of each of the fluids throughout the domain. With this method, the interface lies within a control volume with a liquid volume fraction that ranges from 0 to 1. Its main advantage is that mass is correctly conserved and it can be applied on any mesh. However, the interface normal vector and curvature are difficult to calculate, resulting in a low-quality interface.

Several authors performed multiple VOF simulations onto this kind of impact. Coppola et al. [19] and Rocco et al. [47] analysed the early and intermediate stages of the droplet impact phenomenon, such as the formation of the ejecta sheet subsequent to impact and the early development of the crown. Both simulations were able to capture the bubble entrapment of the gas. This peculiarity consists of very small bubbles of gas being trapped between the droplet and the liquid film. Also, it was concluded that, despite two-dimensional results agreeing well with both numerical and experimental results, this phenomenon is essentially three-dimensional and axisymmetric crowns developing from this kind of impact on nature are very unlikely. Therefore, these articles will serve as a reference in developing codes that better simulate the 3D complexity. Nikolopoulos et al. [48] also investigated the initial stages of the impingement. The axisymmetric numerical simulation was proven to be accurate regarding experimental results, as well as predicting several details, such as bubble entrapment, air and liquid jetting and capillary waves.

Another popular method is the Level Set Method (LSM) [49]. The interface of this method is represented implicitly as a zero level set of a continuous function. It is rather convenient since the interface can be calculated with a better resolution compared to the VOF method. Nevertheless, this method has no conservative properties, which means that a better interface is obtained at the expense of reduced accuracy in conserving mass. Achieving mass conservation, as well as capturing the interface accurately, is obtained by using the coupled level set and volume of fluid (CLSVOF) method. This method, proposed by Sussman and Puckett [50], uses the LSM to compute the geometric properties at the interface, while the volume fraction is calculated using the VOF method. Numerous authors [9, 29, 51, 52] simulated droplet impact using this method, which were validated by experimental results.

There are other methods that, unlike VOF or LSM, do not need to track the interface between the liquid and the gas, such as the Boundary Integral Method (BIM) for scalar velocity potential [53] or the Lattice-Boltzmann Method (LBM) [54, 55, 56].

Several other methods have been on the uprising recently, particularly the Lagrangian particle methods. This includes the Smooth Particle Hydrodynamics (SPH) method [57, 58, 59] and the Moving Particle Semi-implicit (MPS) method [60, 61]. Generally, particle methods offer some advantages when comparing to grid-based methods. Since they are relatively easy to implement and are inherently well suited for simulating large deformation flows and fragmentation problems due to their mesh-free formulation, particle methods are exceptionally good in simulating single droplet impact onto liquid films.

There are also methods in which the Navier-Stokes equations are solved directly without the need for a turbulence model. These are Direct Numerical Simulations (DNS) and Tryggvason et al. [62] uses a front-tracking method for this kind of simulations. This method consists on treating the different phases together by solving one set of equations for the entirety of the computational domain. There is some developed work in terms of front-tracking methods [63, 64]. However, the computational cost of DNS is extremely high, even at low Reynolds Numbers. In most industrial applications, the computational resources required by DNS exceed, by far, the capacity for most of the powerful computers that currently exist.

Chapter 3

Numerical Setup

This chapter will introduce the numerical method, as well as the problem conditions and the numerical setup. The first section introduces multiphase flows and the different challenges that numerical simulations have faced over the recent years. Over this section, the VOF model is thoroughly described in terms of its limitations, governing equations and implemented models regarding surface tension and wall adhesion.

The second section describes the physical properties of the fluids and the characteristics of the six visualized phenomena, which includes the impact velocity, the droplet diameter and the dimensionless thickness. An experimental arrangement and a MATLAB algorithm are also detailed to obtain the contact angles of the different fluids. These angles were required in order to complement the numerical model.

The third section refers to the numerical analysis of the physical phenomena regarded as droplet impact. The geometry and the correspondent mesh, general settings, adopted models, boundary conditions, solution approach and initialization are carefully presented.

The fourth and final section exhibits the grid independence study for the current numerical model. This study is required to verify when the solution is independent on the grid size. Independence is achieved when finer meshes do not affect the numerical solution.

3.1 Volume of Fluid (VOF) Model

3.1.1 Introduction

According to ANSYS Fluent [65], the first step in solving any multiphase problem is determining the flow regime of the problem. These regimes are defined by the different interaction between phases, such as gas-liquid, gas-solid, liquid-liquid, among others. The phenomena regarding droplet impact are defined as a flow of discrete fluid droplets in a continuous gas, which is considered a liquid-gas interface. There are a few important aspects to recognize regarding this kind of interface, such as the contact angle and the surface tension, which are reviewed over this chapter.

Subsequent to defining the flow regime, there are several ways on how to approach multiphase modelling. Currently, two basic approaches to dynamic flow simulations of two-phase gas-liquid flows have been discussed: the Euler-Lagrange approach and the Euler-Euler approach.

The Lagrangian discrete phase model follows the Euler-Lagrange approach. This approach consists in treating the gas-phase motion as a continuum by solving the Navier-Stokes equations, while the dispersed liquid-phase is solved by tracking a large number of particles throughout the calculation flow field in a Lagrangian reference frame. Due to the fact that the particle trajectories are computed individually during the entire process, this model is particularly favourable

for modelling spray dryers, coal and liquid fuel combustion. The dispersed phase and the Lagrangian droplet dispersion models are thoroughly detailed in Silva [18]. In the Euler-Euler approach, both the liquid-phase and the gas-phase are treated as continuum. However, since the volume of a phase cannot be occupied by other phases, the concept of volume fraction is introduced. These volume fractions are assumed to be continuous functions of space and time and their sum is equal to one.

Since there is a considerable interest in treating the different phases as continuum, and no particular significance in tracking disperse particles, the Euler-Euler approach is adopted for the numerical model. Currently, ANSYS Fluent 19.0 provides three different models for this kind of simulations: The Volume of Fluid (VOF) model, the Eulerian model and the Mixture model. Choosing a model that correctly adapts the physical problem might be a complication. Overall, the VOF model is appropriate for stratified or free-surface flows, as well as tracking the interface between the fluids, while and Eulerian and the Mixture model are more convenient for flows in which the phases mix or separate. Therefore, the VOF model was adopted for the numerical simulation.

3.1.2 Governing Equations

Regardless of the flow properties, ANSYS Fluent [65] solves mass and momentum conservation equations. Since there is a predefined grid that does not move with the interface, the conservation equations are presented on an inertial (non-acceleration) reference frame. The equations for mass and momentum conservation are displayed by the equations 3.1 and 3.2, respectively:

$$\frac{\partial \rho}{\partial t} + \nabla \cdot \left(\rho \vec{U}\right) = S_m \quad (3.1)$$

$$\frac{\partial}{\partial t}\left(\rho \vec{U}\right) + \nabla \cdot \left(\rho \vec{U}\vec{U}\right) = -\nabla p + \nabla \cdot (\overline{\overline{\tau}}) + \rho \vec{g} + \vec{F} \quad (3.2)$$

where S_m refers to a mass source added to the continuous phase from the dispersed second phase, such as changes in phases (vaporization of liquid droplets, for example), $\vec{U}$ is the velocity vector, p is the static pressure, $\overline{\overline{\tau}}$ is the stress tensor, $\rho\vec{g}$ is the gravitational body force and $\vec{F}$ are the external body forces. The stress tensor, $\overline{\overline{\tau}}$, is defined by equation 3.3:

$$\overline{\overline{\tau}} = \mu \left[\left(\nabla \vec{U} + \nabla \vec{U}^T\right) - \frac{2}{3}\nabla \cdot \vec{U} I\right] \quad (3.3)$$

where I is the unit tensor and the term $\left(2/3\nabla \cdot \vec{U} I\right)$ refers to the volume dilation.

Equations 3.1 and 3.2 are the general form of mass and momentum conservation. Later on, these equations simplify due to several assumptions, such as incompressibility. In order to track the interface between different phases, the solution of this equations must be coupled with some model capable of following the deforming liquid-gas interface. The VOF model tracks the interface between the phases by coupling the solution of the continuity equation with the volume fraction equation for two or more phases. For an undefined number of phases, the volume fraction is defined by equation 3.4:

$$\frac{1}{\rho_q}\left[\frac{\partial}{\partial t}\left(\alpha_q \rho_q\right) + \nabla \cdot \left(\alpha_q \rho_q \vec{U}_q\right) = S_{\alpha_q} + \sum_{p=1}^{n}\left(\dot{m}_{pq} - \dot{m}_{qp}\right)\right] \quad (3.4)$$

where S_{α_q} refers to the source term, $\dot{m}_{pq}$ *and* $\dot{m}_{qp}$ is the mass transfer from phase p to phase q and from phase q to phase p, respectively, α_q represents the volume fraction for each phase and the subscript q and p describes the q and p phase, respectively. In order to understand this equation, an explanation regarding material properties and the concept of volume fraction is necessary.

Identifying each phase separately requires a function that represents the volume fraction over the computational grid. Since the VOF model specifies that the different phases are inter-penetrating, each phase is represented by the correspondent volume fraction. For every cell displayed on the computational grid, the volume fraction of the q phase, α_q, may vary from 0 to 1, which means that the cell is empty of the q phase if $\alpha_q = 0$ and the cell is full of the q phase if $\alpha_q = 1$. However, if $0 < \alpha < 1$, it means that the cell contains the interface between the q phase and one or more other phases. Since all control volumes must be filled with either a single phase or a combination of two or more phases, due to the fact that the VOF model does not allow for void regions within the computational grid, the sum of all the volume fractions of the different phases inside of each cell must be equal to one, as represented by equation 3.5:

$$\sum_{q=1}^{n} \alpha_q = 1 \quad (3.5)$$

The material properties in the transport equation, ρ and μ, are not constant in all the physical domain and are determined by the presence of the different phases in each control volume. Equations 3.6 and 3.7 present how density and viscosity are defined within the computational grid, respectively.

$$\rho = \sum_{q=1}^{n} \alpha_q \rho_q \quad (3.6)$$

$$\mu = \sum_{q=1}^{n} \alpha_q \mu_q \quad (3.7)$$

Overall, these equations describe general models where several phases coexist. Considering the current physical model, there are several assumptions regarding this kind of phenomenon that simplify the numerical analysis. First of all, a liquid-gas interface defines the two-phase flow, leading to the material properties only depending on the liquid and gas phases. Heat exchanges are neglected during the entire process, which implies that there is no need for an additional equation regarding energy conservation. Compressibility effects are also not taken into account for $M < 0.3$, where M is the Mach number. Therefore, $\partial\rho/\partial t = 0$ and the dilation term of the stress tensor is also negligible. The source terms, S_m and S_{α_q}, as well as the sum term of the volume fraction equation (which refers to the mass flow rate), are equal to 0 due to the fact that there is no mass transfer or physical changes of the different phases during the process.

Acknowledged these assumptions, the governing equations that describe the physical model are presented by equations 3.8 to 3.12. Equations 3.8 and 3.9 express mass and momentum

conservation equations, respectively, equation 3.10 refers to the volume fraction equation, equations 3.11 and 3.12 display volume-fraction-averaged density and viscosity, in the order described.

$$\nabla \cdot \vec{U} = 0 \quad (3.8)$$

$$\frac{\partial}{\partial t}\left(\rho\vec{U}\right) + \nabla \cdot \left(\rho\vec{U}\vec{U}\right) = -\nabla p + \nabla \cdot \left[\mu\left(\nabla\vec{U} + \nabla\vec{U}^T\right)\right] + \rho\vec{g} + \vec{F} \quad (3.9)$$

$$\frac{\partial \alpha}{\partial t} + \nabla \cdot \left(\alpha\vec{U}\right) = 0 \quad (3.10)$$

$$\rho = \alpha_l\rho_l + (1-\alpha_l)\rho_g \quad (3.11)$$

$$\mu = \alpha_l\mu_l + (1-\alpha_l)\mu_g \quad (3.12)$$

3.1.3 Surface Tension and Wall Adhesion

Understanding how surface tension and wall adhesion relate to the current physical model in terms of surface analysis is essential to the numerical simulation. The VOF model allows the user to implement the effects of surface tension between each pair of phases along with the contact angles between the phases and the walls [65].

Currently, ANSYS Fluent 19.0 offers two different schemes to numerically model surface tension: the Continuum Surface Force (CSF) and the Continuum Surface Stress (CSS) models. The simulations presented in this dissertation have been obtained by means of the CSF model due to several reasons. First, the CSF model has a low computational cost and a wide diffusion in many commercial codes, proving to be successful in a variety of physical models. Second, the CSS model provides few advantages over the CSF model for cases involving variable surface tension. Therefore, the CSF model proves to be satisfactory for modelling two-phase flows with constant surface tension.

The continuum surface force (CSF) model, developed by Brackbill et al. [66], computes the effects of the surface tension to the VOF calculations by means of an explicit term in the momentum equation. The surface curvature is computed from the local gradients in the surface normal at the curvature. The normal surface, n, is defined by equation 3.13.

$$n = \nabla\alpha \quad (3.13)$$

The curvature of the interface, κ, may be expressed in terms of the divergence of the unit normal vector to the interface, as represented by equation 3.14:

$$\kappa = -\nabla \cdot \left(\frac{\nabla\alpha}{|\nabla\alpha|}\right) = -\nabla \cdot \left(\frac{n}{|n|}\right) \quad (3.14)$$

and the surface tension force, by means of the CSF method, is represented in a non-conservative form, as displayed by equation 3.15.

$$F_{CSF} = \sigma\kappa\nabla\alpha = \sigma\kappa n \quad (3.15)$$

Brackbill et al. [66] also developed a model to adjust the curvature of the surface tension near walls by defining a contact angle that the fluid is assumed to make when in contact with a wall.

The contact angle is defined as the angle formed by the intersection of the liquid-solid interface and the gas-liquid interface. According to Rioboo et al. [11], wetting is defined as the ability of a liquid to maintain contact with a solid surface. It is specific to the interface where solid, liquid and gas coexist, and the degree of wetting is determined by a force balance between cohesive and adhesive forces. Figure 3.1 describes wetting and non-wetting systems in terms of the measured contact angles, θ_w.

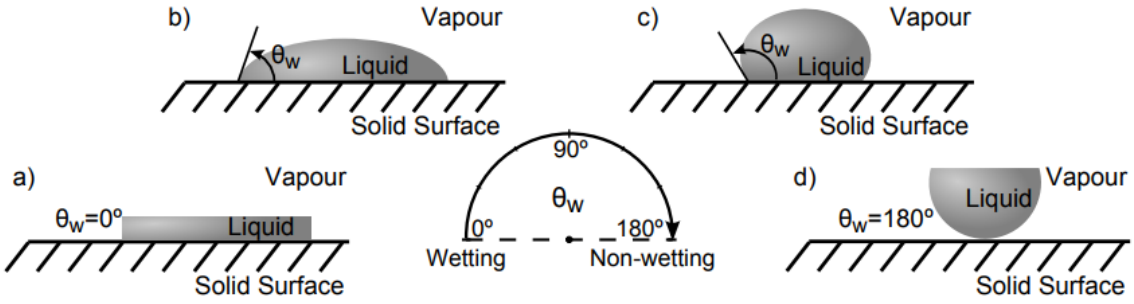

Figure 3.1: Possible contact angles of a drop impacting onto an ideal surface: a) complete wetting; b) partial wetting; c) partial non-wetting; d) complete non-wetting by Rodrigues [67]

If the wetting of the surface is favourable, the fluid will spread over a large area of the surface and the value of θ_w is lower than $90°$. However, if the wetting of the surface is not favourable, the fluid will minimize its contact with the surface and form a compact liquid droplet, where θ_w is greater than $90°$. There are also the complete wetting and non-wetting systems, which relate to $\theta_w = 0°$ and $\theta_w = 180°$, respectively. Complete wetting occurs when the droplet turns into a flat puddle. However, complete non-wetting is practically not possible to occur, considering that the liquid droplet would have no contact with the solid surface. Superhydrophobic surfaces present contact angle values higher than $150°$, barely showing contact between the droplet and the surface, and are the closest to complete non-wetting systems.

Consequently, the VOF model allows to specify the contact angle that the fluid is assumed to make in order to adjust the surface normal in cells near the wall, which is represented by equation 3.16:

$$\hat{n} = \hat{n}_w cos\,(\theta_w) + \hat{t}_w sin\,(\theta_w) \quad (3.16)$$

where $\hat{n}$ is the normal unit, which can also be represented by $\hat{n} = n/|n|$, and $\hat{n}_w$ and $\hat{t}_w$ are the normal and tangential unit vectors to the wall, respectively.

Due to these reasons, enabling wall adhesion along with surface tension on the numerical model grants higher accuracy when comparing to the physical results.

3.2 Flow Configuration

The vertical impact of a single droplet onto a liquid film with the same liquid properties, surrounded by air, is studied numerically. Following the experimental study by Ribeiro [2], four different fluids were taken into account: water, 100% Jet A-1 and 75%/25% and 50%/50% of Jet A-1 and NEXBTL [68], respectively, where Jet A-1 is a type of aviation fuel designed for aircraft powered by gas-turbine engines and NEXBTL is neste renewable diesel, which is a hydrotreated vegetable oil (HVO). The properties of these fluids, such as density, dynamic viscosity and surface tension, are presented in table 3.1.

Table 3.1: Physical properties of density, dynamic viscosity and surface tension of the different fluids. Adapted from Ribeiro [2]

Fluid	ρ $[kg/m^3]$	μ $[mPa.s]$	σ $[mN/m]$
H_2O	1000	1.00	72.0
100% JF	798	1.12	25.4
75% JF/25% HVO	795	1.44	25.5
50% JF/50% HVO	792	1.79	24.6

The different parameters that affect the droplet dynamic behaviour, such as the impact height, the droplet diameter and the non-dimensional thickness, are also considered. The distinct combinations between these parameters provide around 180 cases of study which, in terms of computational analysis, requires an enormous amount of time. However, only six different outcomes, which are spreading, jetting, fingering, crown splash, prompt splash and bubbling, were visualized. Therefore, in order to correlate computational time with the cases of study, only these six different outcomes will be numerically simulated and compared with the experimental results. The following table 3.2 distinguishes the different outcomes in terms of fluid, impact diameter, impact velocity and dimensionless thickness. Table 3.3 displays the dimensionless numbers for the same outcomes.

Table 3.2: Possible outcomes and respective droplet diameter, impact velocity and dimensionless thickness. Adapted from Ribeiro [2].

Outcome	Fluid	$D_0[mm]$	$U_0[m/s]$	h^*
Spreading	75% JF/25% HVO	2.8	1.8	1
Jetting	100% JF	3.0	1.8	1
Fingering	75% JF/25% HVO	2.5	1.8	0.1
Crown Splash	H_2O	3.2	4.1	0.27
Prompt Splash	50% JF/50% HVO	3.1	4.1	0.1
Bubbling	75% JF/25% HVO	3.1	4.1	0.5

It must also be mentioned that the spreading, jetting and fingering outcome display impact velocities around $U_0 = 1.8m/s$ due to the fact that the impact height is $h_1 = 0.175m$ and the crown splash, prompt splash and bubbling exhibit impact velocities around $U_0 = 4.1m/s$ since the impact height, $h_3 = 1m$, is higher than the first three outcomes. Tests regarding the impact height $h_2 = 0.5m$ were not considered for the numerical simulations. The different impact diameters are also obtained by needles with distinct inner diameters.

Despite the droplet impacting onto a liquid film, the surface properties beneath are required,

Table 3.3: Possible outcomes and respective Reynolds, Weber, Ohnesorge and Laplace Numbers. Adapted from Ribeiro [2].

Outcome	Re	We	$Oh \cdot 10^3$	La
Spreading	2751	279	6.069	44793
Jetting	3899	310	4.514	49087
Fingering	2441	247	6.437	39813
Crown Splash	13348	772	2.081	230879
Prompt Splash	5497	1623	7.328	49338
Bubbling	6847	1568	5.783	49323

such as density and, more specifically, the contact angles of the different fluids. The container that supports the liquid film is a perspex container with a density between $\rho = 1.17 g/cm^3$ and $\rho = 1.20 g/cm^3$ [69]. However, there are no reports in the literature concerning contact angles for these fluids onto perspex surfaces, and Ribeiro [2] did not require these values in the experimental study. In order to complement the numerical model with as many physical properties as possible, an experimental study must be conducted to obtain the contact angles for the different fluids.

3.2.1 Contact Angles

The current subsection describes the experimental setup and the procedures for obtaining the different contact angles. Despite being more important on dry rather than on wetted surfaces, implementing the contact angle into the model is required to adjust the normal surface in cells near the wall and, correspondingly, achieving superior results.

Defining the different aspects of the experimental setup is fundamental and measuring the contact angles for the different fluids under the same conditions as Ribeiro [2] is crucial in obtaining proper results. Therefore, by following the same methodology, the experimental structure must be thoroughly elucidated in terms of impact surface, lighting, image capturing and droplet dispensing system.

The impact surface is a topless perspex container of dimensions 200x200x200mm. These dimensions are appropriate for guaranteeing the non-influence of the radial distance in the droplet impact onto liquid films. Since the static contact angle is measured onto dry surfaces, the radial distance is irrelevant and a smaller container would suffice the needs. However, using the same container as Ribeiro [2] allows correlating the contact angle measurements with the experimental results. The primary function of the illumination is not only providing uniform lighting but also producing a contrast between the droplet and the background. This allows for better imaging in terms of visualization and it is required for the MATLAB algorithm, which will be specified in this section. The image capturing relies on a Photron FASTCAM mini UX50 camera with a 1.3 megapixel image resolution and a Macro Lens Tokina AT-X M100 AF PRO D. With an image resolution of 1280x1024, the camera and the lighting allowed for an acceptable imaging. The droplet dispensing system did not suffer any changes in terms of the experimental arrangement. However, only one needle was required to produce droplets considering that, for elongated droplets on smooth surfaces, the contact angle depends entirely on the materials involved [70]. Several impact heights were also tested to verify if the contact angle was depen-

dent with the impact velocity, which proved to affect the dynamic contact angle but not the static contact angle after a certain period after impact [71].

Following the experimental arrangement, acquiring images of the droplet after impact is necessary for the different fluids. However, ensuring that the droplet is stationary when the image is acquired is a must in measuring the static contact angles. It was observed that, for the water, $t = 200ms$ after impact, the droplet was stationary and did not display any change. Therefore, $t = 200ms$ was the difference between the impacting droplet and the image acquisition. Figure 3.2 represents the water droplet after that period. However, it was not possible to obtain the static contact angles for the remaining fluids. These fluids displayed total spreading upon impacting the dry surface and the corresponding images did not allow to measure the static contact angles. Therefore, these angles are approximately equal to $\theta_w = 0°$, with the exception of water.

Prior to measuring the static contact angles, the MATLAB algorithm written by Ribeiro [2] must be adapted for the experimental procedure. In general, the adapted algorithm behaves in a similar way to the original code. Nevertheless, certain details have to be mentioned to comprehend how the angles were measured.

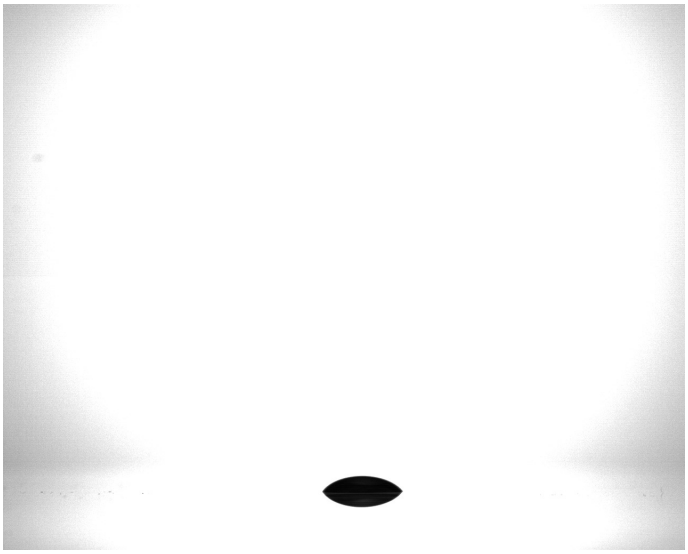

Figure 3.2: Stationary H_2O droplet $t = 200ms$ after impact.

At first, subtracting the background to the figure with the droplet allows obtaining an image with the static droplet only. Formerly, transforming the image into binary and filling the area within the droplet is performed. So far, the algorithm execution is equal. From this point forward, both the droplet and the associated reflection emerge from the figure, as noticed in figure 3.2. In order to measure the static contact angle, the line that separates the droplet and its reflection was used to remove the area under that same line, withdrawing the reflection. Using this method allows to obtain the static droplet over the surface line and, consequently, the image is now arranged to measure the respective contact angles. Figure 3.3 displays the static droplet subsequent to the execution of the algorithm.

The final step requires defining a tangent line between the droplet and the surface underneath, as presented by figure 3.1. By means of modifying the MATLAB algorithm, it is possible to count the pixels on the interface between the droplet and the gas and, by this method, mark a proper and rigorous tangent line in one of the sides of the droplet. Several tests for water

Figure 3.3: Droplet after the implementation of the algorithm.

were considered to obtain reliable results. Table 3.4 presents the static contact angles for the different fluids onto the perspex surface.

Table 3.4: Static contact angles onto a perspex surface for the different fluids

Fluid	$\theta_w[^\circ]$
H_2O	50.3
100% JF	≈ 0
75% JF/25% HVO	≈ 0
50% JF/50% HVO	≈ 0

3.3 Numerical Modelling

3.3.1 Geometry and Meshing

Creating a geometry and a mesh that can adjust to the physical problem is the first step in obtaining reliable solutions. ANSYS Fluent 19.0 currently provides two different software to create geometry: *SpaceClaim* and *DesignModeler*. The latter software is best suited for this analysis due to an accessible graphical user interface and, since the geometry is rather simple, it is more advantageous choosing it.

First of all, the analysis is defined as two-dimensional (2D) axisymmetric assumption. Overall, 2D simulations are less resource consuming and can adequately resolve the droplet impact phenomenon, despite its three-dimensional (3D) nature.

Figure 3.4 displays an initial representation of the geometry and mesh for the physical model. The geometry of the current model is represented by an equiangular quadrilateral. The quadrilateral sides are defined as $V1$ and $H2$, which are the grid radial distance and the grid height, respectively. Depending on the side length, this geometry is displayed as a rectangle or a square. The size values for $V1$ and $H2$ are correctly defined over the radial independence study on an upcoming chapter.

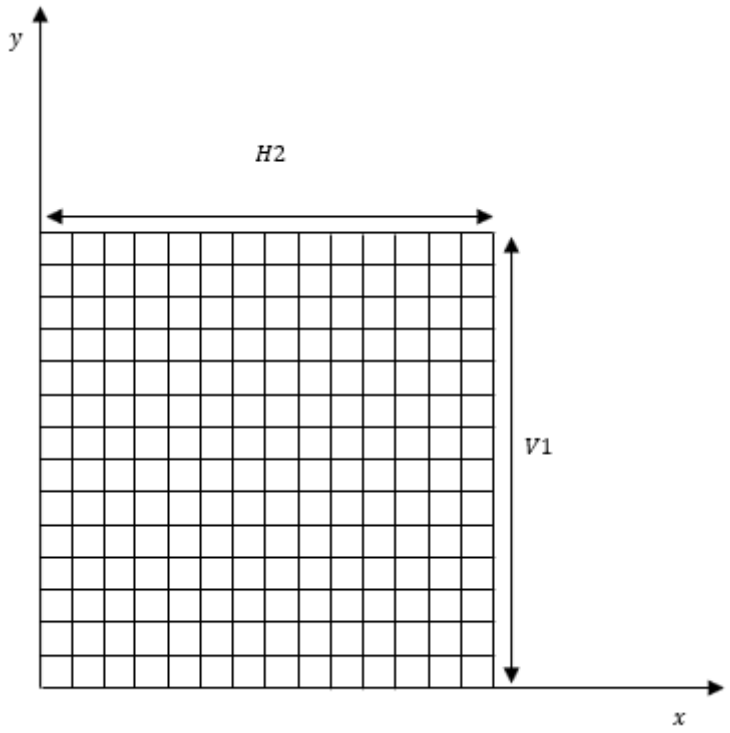

Figure 3.4: Initial representation of the geometry and mesh of the physical model.

In terms of the mesh, the one that better adjusts for the corresponding geometry is a quadrilateral one. Therefore, it is possible to obtain a structured grid by face meshing the geometry with quadrilaterals and sizing the edges for a proper mesh distribution.

3.3.2 General Settings

This subsection allows to check the current mesh and define the gravitational acceleration, as well as different solvers regarding time, velocity and space.

It is generally a good idea to check the mesh before getting started with the problem setup in order to detect any mesh trouble. The current mesh, as expected, presents no issues. The respective details about domain extents and statistics related to cell volume and face area are presented when grid independence is performed.

The solver chosen for this model is the pressure-based solver. Overall, both the pressure-based and the density-based solvers can be used for a broad range of flows, where the pressure-based one is traditionally applied for incompressible and mildly compressible flows and the density-based one, on the other hand, was originally designed for high-speed compressible flows. Regardless of these reasons, the pressure-based solver is the only available option since the density-based solver is not compatible with multiphase modelling.

Choosing the velocity formulation that results in most of the flow domain having the smallest velocities leads to a more accurate solution by reducing the numerical diffusion. The relative velocity formulation is appropriate when most of the fluid in the domain is rotating, whereas the absolute formulation is preferred where the flow in most of the domain is not rotating, hence choosing the absolute velocity formulation for the simulation.

The main contrast between steady-state and transient formulations relies on the time interval. If the interest is the steady conditions reached after a relatively long time interval, then steady-state formulation should be considered. However, since the main purpose of this thesis is verifying the liquid-gas interface during the droplet impact phenomenon, where the solution is not steady, the transient formulation is the leading option.

As already mentioned, 2D simulations can save processing time and conserve computational resources. Considering the 3D nature of the phenomena, the optimal way to represent the physical model in 2D consists of assuming an axisymmetric model. This model assumes that a 3D model can be generated by revolving a 2D section 360° about an axis. Comparing to planar, which only indicates that the problem is 2D, or the axisymmetric swirl, which involves a circumferential component of velocity, the axisymmetric model adapts particularly well to the physical phenomena. However, there are a few peculiarities when performing axisymmetric simulations. Since ANSYS Fluent 19.0 predefines the axis of symmetry as the x-axis, the geometry must lie on the positive y-axis of the x-y plane, where the x direction is axial, the y direction is radial and the z direction is the circumferential direction. Hence, defining the gravitational acceleration in the axial direction, specifically with a positive orientation, is necessary.

3.3.3 Adopted Models

The models provided by ANSYS Fluent allow representing almost any physical phenomena that we may encounter in nature, such as multiphase, heat exchange, turbulence, radiation, etc. Specifically for multiphase models and droplet impact interactions, the applied models are relatively simple.

First, the VOF model is enabled. As explained in section 3.1, this multiphase model specifies the number of Eulerian phases which, in this case, consists of two: the primary phase and the secondary phase. It is more convenient to define the primary phase as the gas phase and the secondary phase as the liquid phase since the gas occupies most of the mesh and the liquid will be patched later on. The gas material is air with the following properties: $\rho = 1.225 kg/m^3$ and $\mu = 1.789 \times 10^{-5} kg/m.s$. The liquid phase properties have been already presented on section 3.2. Interactions between phases are also implemented, such as the CSF model for the surface tension and the wall adhesion for the contact angles. There are also explicit and implicit ways of formulating volume fraction parameters. In general, the explicit formulation is non-iterative and time-dependent and it can only be used with the transient solver. It exhibits better numerical accuracy when compared to the implicit formulation, however, the time step is limited by the Courant Number. This number, which is based on the Courant-Friedrichs-Lewy (CFL) condition, expresses that the distance that any information travels during the time step length within the mesh must be lower than the distance between mesh elements. It must not exceed a certain maximum value, otherwise, the numerical scheme will become unstable and the solution diverges. This maximum value differs with the method used to solve the discretised equations, as well as the explicit and the implicit formulation. The Courant Number is expressed by the equation 3.17 for the n-dimensional case, where Δt refers to the time step, U_{x_i} refers to the magnitude of the velocity in a certain direction and Δx_i is the length interval in a certain direction as well.

$$C = \Delta t \sum_{i=1}^{n} \frac{U_{x_i}}{\Delta x_i} \leqslant C_{max} \quad (3.17)$$

On the contrary, since the implicit formulation is more suited for steady-state solutions if there is no interest in the intermediate transient flow behaviour, then the explicit formulation for the volume fraction is adopted. Lastly, if large body forces exist in multiphase flows, such as gravity or surface tension forces, enabling implicit body force formulation improves solution convergence by accounting for the partial equilibrium of the pressure gradient and body forces in the momentum equations.

The viscous model adopted is a laminar model. Despite the large number of options that range from inviscid models to turbulent models, such as k-epsilon or k-omega, there is no need to implement turbulence modelling. Due to these reasons, the laminar model complements the study rather well.

There are several other models, such as heat exchanger, species, discrete phase, among others. None of these models was considered since the main focus is the physical interaction between the two phases and not the chemical interactions that models, such as the heat exchanger or the species, may provide. The energy equation is also not enabled since there are no heat exchanges during the entire process.

3.3.4 Boundary Conditions

The boundary conditions specify how the flow develops within the boundaries of the physical model. They are a critical component when simulating any type of numerical models since poorly defined boundary conditions can have a significant impact on the solution. Figure 3.5 exhibits the different boundary conditions for the physical model.

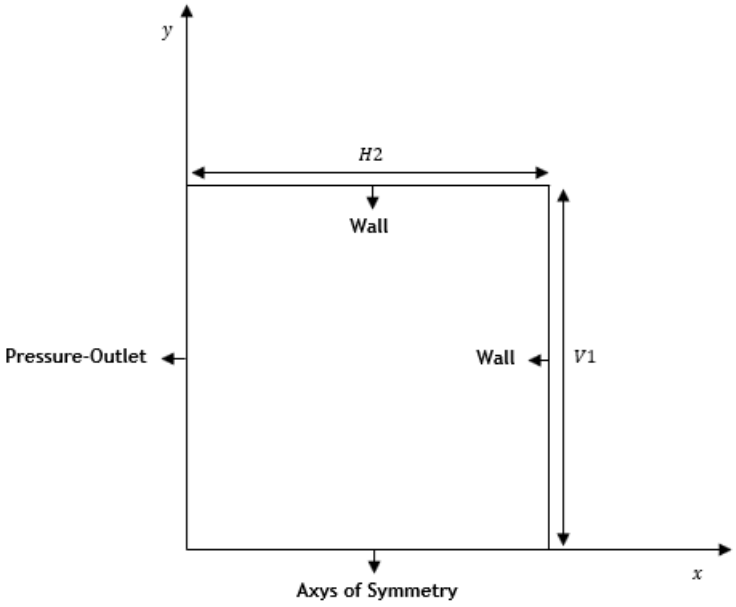

Figure 3.5: Boundary conditions of the physical model.

As mentioned on subsection 3.3.2, ANSYS Fluent predefines the x-axis as the axis of symmetry in axisymmetric models. This axis matches the vertical trajectory of the droplet and it is parallel to

the gravitational acceleration, $||\vec{g}|| = ||\vec{g_x}|| = 9.81 m/s^2$. This implies that the droplet will impact the right boundary, where the liquid film exists. In terms of visualization, this may be considered unusual, since the liquid film is normally on the bottom boundary. The optimal solution is, when presenting the final results, rotating the figures 90° clockwise so that the comparison between the numerical analysis and the experimental results may be of ease. However, for this chapter, the geometry and the axis orientation will remain the same.

There are four different boundary conditions that define the physical model. The bottom boundary consists of the axis of symmetry and it is used as the centerline of an axisymmetric geometry. The right and top boundary are defined as the bottom and the radial wall, respectively, where both walls are stationary and the no-slip shear condition is applied. Since wall adhesion is enabled, the bottom wall will have a correspondent static contact angle, depending on the fluid. However, since the surface tension effects are ignored between the radial walls and the interface, the static contact angle on the radial wall is $\theta_w = 90^\circ$. The left boundary is a pressure-outlet boundary with a static gauge pressure of $p_{gauge} = 0Pa$ which, in combination with an operating pressure of $p = 1atm$, correlates to the topless perspex container as a free boundary condition.

3.3.5 Solution Approach

Choosing between several methods on how they numerically behave and if they are capable of accurately representing physical models is a challenge. ANSYS Fluent 19.0 supports different solvers, such as pressure and density-based solvers, different schemes considering pressure-velocity coupling, as well as spatial and temporal discretization. Finding an ideal balance between these solution methods is rather difficult and involves a somewhat deep knowledge about equation discretization, solvers, etc.

The pressure-velocity coupling method adopted was the Fractional Step Method (FSM). The reasoning behind choosing this method over other general methods, such as Pressure-Implicit with Splitting of Operations (PISO) or Semi-Implicit Method for Pressure-Linked Equations (SIMPLE), lies on several reasons. First, for time-dependent flows, there are two approaches on how to control the splitting error, which are the iterative time-advancement (ITA) scheme and the non-iterative time-advancement (NITA) scheme. The NITA scheme is often advantageous compared to the iterative schemes as it is less Central Processing Unit (CPU) expensive and, even though smaller time steps must be used when running NITA simulations, the total CPU expense is smaller when compared to iterative schemes. However, if NITA schemes lead to convergence difficulties, then iterative schemes should be used instead. Even so, there were no convergence issues for the numerical model. For NITA schemes, there are two different methods: PISO and FSM. Overall, these schemes have similar characteristics and the results for the testing of these different schemes proved to be mostly identical. However, the PISO scheme proved to be more CPU expensive than the FSM and, consequently, more time was required to run the same number of iterations. Due to these reasons, the FSM is adopted for the current model.

ANSYS Fluent allows the user to choose the discretization scheme for the convection terms of each governing equation. The spatial discretization schemes for gradient, pressure, momentum and volume fraction offer alternative options on how to store discrete scalar values at the cell centres.

Gradients are needed not only for constructing scalar values at the cells, but also for velocity

derivatives and secondary diffusion terms. Green-Gauss Cell Based, Green-Gauss Node Based and Least Squared Cell Based are the different methods for computing gradients. For this model, no particular differences have been noticed for the various methods. Therefore, the Least Squared Cell Based method is adopted, since it is the default method that ANSYS Fluent provides.

For VOF and multiphase models, only Pressure Staggering Option (PRESTO!) and body-force-weighted schemes are available for the pressure interpolation. Neither of these schemes is particularly effective for the model, as both seem to adapt quite appropriately. By retaining the default selection, PRESTO! is the selected scheme for pressure interpolation.

Choosing a discretization scheme for the momentum is relatively difficult due to the fact that the numerical results differ quite a lot from different momentum schemes. For the fractional step method, five different schemes for momentum are available: First-order upwind scheme and power-law scheme, which are first-order schemes, second-order upwind scheme, which is second-order, and Quadratic Upstream Interpolation for Convective Kinematics (QUICK) and Monotonic Upwind Scheme for Conservation Laws (MUSCL) schemes that consist in third-order schemes. Generally, the higher the order, the more accurate the results are and the more CPU expensive the numerical simulations are as well. Therefore, as stated previously, finding the balance between accuracy and time is necessary. Initially, tests were performed for first-order schemes. Overall, convergence is rather easy to achieve. However, when considering the number, size and ejection time of secondary droplets, the first-order schemes were not capable of accurately predicting the secondary atomization and, as a result, errors such as fewer secondary droplets or late ejection times would arise. Consequently, the first-order schemes were disregarded for the current model. When simulating second-order schemes, convergence was more complex. Once the droplet impacted on the liquid film, and secondary atomization would occur, the Courant number and the overall residuals would increase dramatically and lead to divergence. By adjusting the quadrilateral mesh size and the correspondent time step, it was possible to reduce the Courant number and avoid divergence. The specifics regarding mesh and time step are approached in the grid independence section. Once convergence was achieved, testing how the second-order upwind scheme developed over time was crucial to verify if no higher scheme orders were required. This scheme proved to be quite consistent and presented decent results but, for comparison terms, the third-order schemes were also evaluated. For third-order schemes, QUICK and MUSCL are available, where the QUICK scheme is typically more accurate for quadrilateral and hexahedral meshes and the MUSCL scheme is applicable to arbitrary meshes. These schemes, due to its higher-order accuracy, have the potential to improve spatial accuracy by reducing numerical diffusion, most significantly for three-dimensional flows, and can be far more superior than second or first-order schemes if applied correctly. As verified on the second-order schemes, convergence was also an issue, and by reducing the Courant number by means of acquiring a high-quality grid and the correspondent time step, it was possible to avoid divergence and converge the simulation. Subsequent to running several simulations, the schemes that best suited the model were the QUICK and the MUSCL schemes. These showed to be remarkably tough to manipulate but the obtained results, in qualitative terms, were exceptional. These are not only capable of accurately predicting secondary atomization but also predict the crown diameter and height development rather successfully. Despite being rather similar, the MUSCL scheme seems more CPU expensive and the QUICK scheme is more appropriate for quadrilateral grids. For these reasons, the QUICK scheme is the adopted scheme for momentum discretization.

The volume fraction formulation and the interpolation near the interface require that convection and diffusive fluxes through the control volume faces be computed and balanced with source terms within the control volume itself. When the volume fraction explicit formulation is used, there are four available schemes that can reconstruct the liquid-gas interface: the geometric reconstruction scheme (Geo-Reconstruct), the Compressive Interface Capturing Scheme for Arbitrary Meshes (CICSAM), the Compressive scheme and a modified version of the High-Resolution Interface Capturing (Modified HRIC) scheme. While the CICSAM, Modified HRIC and the compressive schemes are less computationally expensive than the Geo-Reconstruct scheme, the interface between the liquid and the gas phase will not be as sharp or accurate as the one predicted by the Geo-Reconstruct scheme. Since the Geo-Reconstruct scheme is commonly used whenever the interest relies upon the time-accurate transient behaviour of the VOF solution, which relates to the droplet impact interaction and the secondary atomization, this scheme is crucial to capture the interface between the phases.

Lastly, the NITA solver enables the control of the non-iterative solver relaxation factors for momentum and pressure. These factors exist due to the non-linearity of several equations solved by ANSYS Fluent and it is necessary to control its change along with the iterations. Generally, these factors aid with convergence by not allowing greater changes of the scalar values between iterations and, therefore, avoiding divergence. For most flows, these values do not require modification, and the default values of the pressure and momentum relaxation factors are set to 1. By numerically simulating the current model, with a certain grid, time step, solution methods and controls, it was demonstrated that convergence could be achieved by maintaining the relaxation factors default values, and decreasing these values would not be impactful in the simulations.

3.3.6 Initialization

As the last step of the numerical modelling, initializing the solution and patching the different volume fraction phases and respective velocities are required to recreate the experimental setup.

Before running the calculations, the flow field must be initialized in the entire domain. Standard initialization allows to specify all the variables directly such as velocity, pressure, temperature, etc., and the hybrid initialization solves the Laplace equation to produce a velocity field suitable for complex geometries and a pressure field which smoothly connects high and low-pressure values in the numerical domain where no initial values are required. Overall, the standard initialization fits comparatively well onto the domain by implementing all the initial values, such as impact velocity and volume fraction. Computing from a certain zone within the computational domain, such as the pressure-outlet boundary or the walls, does not affect the overall calculation and, therefore, computing from all-zones allows FLUENT to compute and update the initial conditions over the domain and the boundary conditions. The reference frame did not really have an influence when iterating the solution, so the default option remains as the relative to cell zone option. The initial values, such as gauge pressure, axial velocity, radial velocity and the liquid-phase volume fraction are all equal to 0, meaning that the computational domain is initially defined as the gas-phase with no gauge pressure and with no initial velocity.

Subsequent to the solution initialization, patching the liquid-phase onto the computational domain is the following step. At first, registering the liquid droplet and the liquid film is required.

A register is a group of cells that are marked for coarsening/refinement. The ability to patch values in cell registers gives the flexibility to patch different values within different cell zones, allowing to mark the cells in terms of physical location, cell volume, a particular variable, etc. By this means, there are two registers that need patching in the numerical model: the liquid droplet and the liquid film.

After registering the different zones, patching the volume fraction for the liquid droplet and the liquid film is necessary prior to any other variables, such as the impact velocity. Therefore, by selecting the two different zones and a volume fraction value of 1, the patching of the volume fraction for the droplet and the liquid film is complete. The physical location of the droplet and the liquid film correspond to the moment of impact, where $t = 0ms$. The final detail for patching is the impact velocity of the droplet. Since the values of the impact velocity are described by Ribeiro [2], patching the liquid droplet with an axial velocity equal to the droplet impact velocity is the patching final step. As mentioned on the subsection 3.3.2, the final solution will suffer a $90°$ clockwise rotation and a symmetry over the x-axis for an improved visualization and comparison. Figure 3.6 displays the droplet and the liquid film at the moment of impact.

Before running the calculations, defining a time step is crucial. Initially, an explicit time stepping scheme is adopted for the formulation to maintain time accuracy over the numerical simulation. This particular scheme allows the user to define a global time step, which implies that the same time step will be employed for the overall simulations. Since this is an explicit scheme, it is necessary to adjust the time step in terms of the Courant Number. For this numerical simulation, the maximum Courant Number was set to $C_{max} = 0.5$, as it was observed that, for higher values, the solution would start to diverge. By these means, the time step adopted to maintain the Courant Number below the maximum allowed value was $\Delta t = 1 \cdot 10^{-6} s$. This value was reasonable for the entirety of the numerical simulation to control the Courant Number and to ensure convergence.

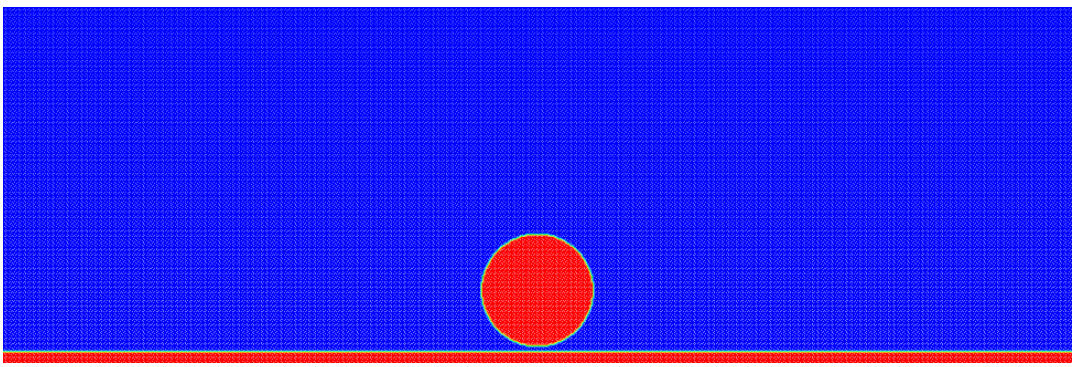

Figure 3.6: Visual representation of the droplet and the liquid film for $t = 0ms$.

3.4 Grid Independence Study

The quality of the mesh and the time step plays a significant role in obtaining accurate and valid numerical results. When solving any physical model numerically, the solution should not be affected by grid size. The grid independence study ensures that the solution is independent for a certain grid size, meaning that finer meshes will not affect the overall simulation.

There are quite a few approaches when performing grid independence tests for this kind of phenomena. Measuring a particular characteristic of the droplet impact, such as crown height, diameter or the number of secondary droplets are several examples of tracking a certain parameter for this model. Since this is a 2D axisymmetric model, defining the independence study as an estimation of the secondary droplets is inaccurate. The formation of secondary droplets is specifically dominant in 3D simulations due to the asymmetry of the phenomena and, for this reasoning, this method does not comply with the numerical simulation. Between the height and the inner or outer diameter of the crown, and following the mesh refinement study performed by Liang et al. [29], the grid independence study is based on the inner diameter of the respective crown. Determining the inner diameter is rather simple due to the fact that the mesh size is previously defined for each grid and, therefore, defining a certain height where the inner diameter measuring occurs is crucial in achieving reliable results. Figure 3.7 shows the grid independence study.

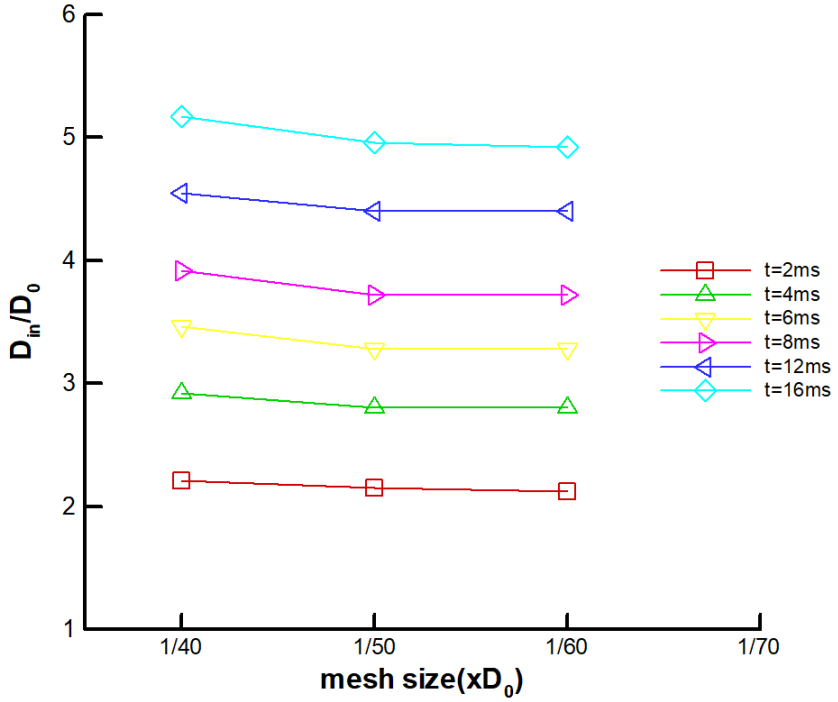

Figure 3.7: Mesh refinement study of the numerical model for the inner diameter of the crown, non-dimensionalized by the droplet diameter, as a function of the mesh size.

The conditions referring to this study relate to one case of study by Ribeiro [2] where the fluid is water, $D_0 = 4.0mm$, $h^* = 1$ and $U_0 = 4.2m/s$. This case is especially appropriate for this grid independence study since, during the impact development, the crown is relatively thick and high, allowing for more accessible measurements of the inner diameter. The inner diameter of the crown, D_{in}, is analysed for $t = 2, 4, 6, 8, 12$ and $16ms$. A coarse, medium and fine were tested for $1/40$, $1/50$ and $1/60$ of the droplet diameter, respectively. The grid independence is obtained when no further mesh refinement makes significant changes in the numerical results. It was verified that, between the medium and fine mesh, which relate to the $1/50$ and $1/60$ of the droplet diameter, respectively, the maximum relative error in the diameter is 1.40%. For these reasons, the mesh size equal to $1/50$ of the droplet diameter is adopted for the current simulations. Figure 3.7 displays the variations of the outer crown diameter, non-dimensionalized by the droplet diameter, with the mesh refinement.

Figure 3.8 also displays the grid independence study, not as a function of the mesh size, but as a function of the dimensionless time. It is possible to verify that there barely is a distinction between the results of $1/50$ and $1/60$ of the droplet diameter, as the corresponding lines practically overlap. This figure is a distinct form of displaying the mesh refinement study presented on figure 3.7.

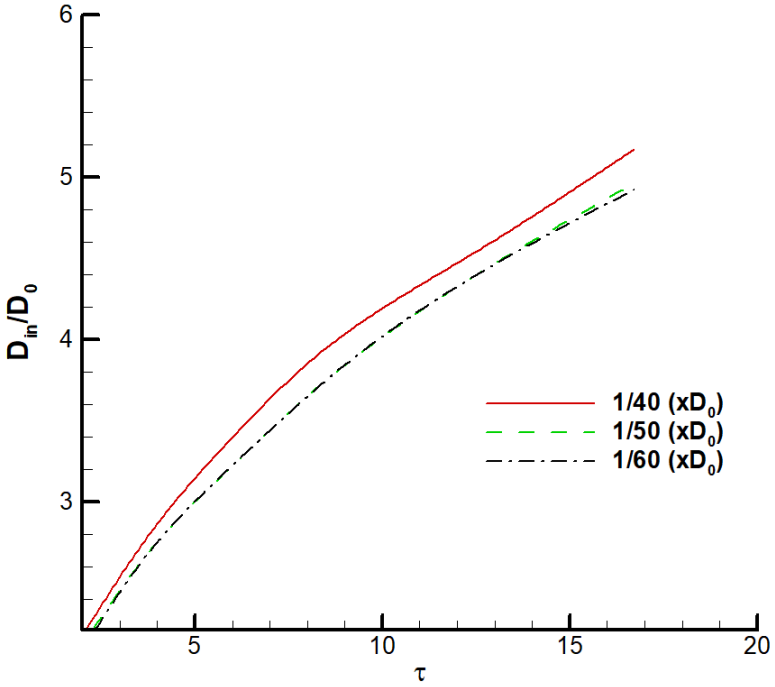

Figure 3.8: Mesh refinement study of the numerical model for the inner diameter of the crown, non-dimensionalized by the droplet diameter, as a function of the dimensionless time.

Chapter 4

Results and Discussion

This chapter introduces the numerical results and the comparison with the different experimental outcomes. Overall, the phenomena visualization is similar despite some variations that need further discussion.

The first section presents each of the different observed phenomena: Prompt Splash, Crown Splash, Spreading, Jetting, Fingering and Bubbling. A comparison between the experimental and the numerical analysis is also presented.

The second section introduces a quantitative comparison of these results and the radial independence study, which is required to avoid over-dimensioned meshes. The final section summarizes this chapter in terms of the outcomes and validation of the results.

4.1 Visualization

Various characteristics regarding the visualization and comparison of the results must be conferred prior to exhibiting the figures. First, the experimental and numerical figures were adjusted in terms of size to assist on an easier comparison between the results. For the numerical results, these are essentially distinguished by the red and the blue colour, where the red colour defines the liquid phase and the blue colour the gas phase. On the liquid-gas interface, it is observable a variety of colours, such as yellow and green, which are zones where the liquid and the gas phase coexist. Experimental and numerical results are displayed side-by-side for the six different outcomes for characteristic moments that define these types of impact, such as splashing, crown development, bubble entrapment, etc.

4.1.1 Prompt Splash

The prompt splash is a type of splashing that occurs at the very early stages of the impact, usually for $t << D_0/U_0$, and is characterized by the generation of tiny droplets from the tip of the lamella at the contact line of the spreading liquid-substrate. Figure 4.1 displays the experimental and numerical results of the prompt splash phenomenon for $D_0 = 3.1mm$, $U_0 = 4.1m/s$ and $h^* = 0.1$.

At first, the droplet prior to impact is presented, for $t = 0ms$. These frames were adopted as the initial frame for all the six cases since they represent the exact moment before the droplet connects with the liquid film. Once the droplet impacts, due to the high impact velocity, the ejecta sheet is formed and it disintegrates into tiny secondary droplets, as is observed for $t = 0.5ms$.

With the development of the initial impact, the crown starts to expand and, for $t = 1.5ms$, the crown height and diameter show advancement in terms of height and radial distance, respec-

tively. The secondary droplets, previously ejected, advance away from the impact region and additional secondary atomization occurs. The following stages, for $t = 2.5ms$ and $t = 3.5ms$, are similar to the previous one, as the crown continues to grow, both in height and diameter, and the secondary droplets continue to spread. It is also noticeable that the thickness of the crown is relatively low during the different stages of the droplet impact due to the reduced dimensionless thickness, which is consistent with the ejecta sheet being originated from the underlying liquid film and not the liquid drop [22].

Overall, the numerical results are consistent with the available experimental data in terms of the ejection time of secondary atomization and crown development for the prompt splash phenomenon. If, however, the objective is finding out the number of secondary atomization, the 2D axisymmetric model does not provide an accurate solution.

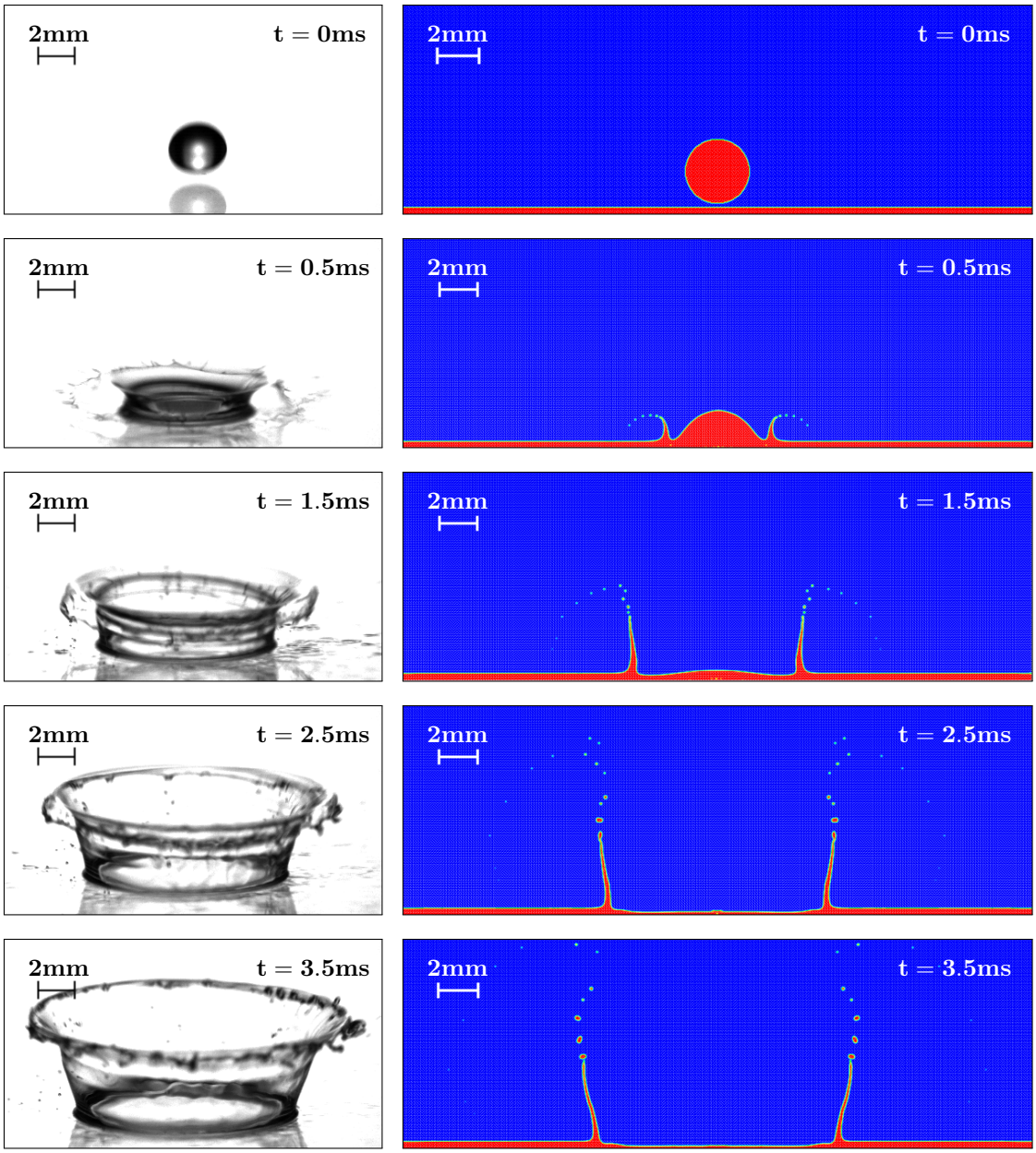

Figure 4.1: Visualization of the prompt splash phenomenon for the 50% JF/50% HVO mixture ($D_0 = 3.1mm$, $U_0 = 4.1m/s$, $h^* = 0.1$): (a) Experimental Results; (b) Numerical analysis.

4.1.2 Crown Splash

Crown splashing is commonly seen on droplets impacting onto liquid films. This phenomenon, unlike prompt splashing, occurs for later stages of the impact when the crown fully develops and secondary droplets are ejected from the rim. These droplets are considerably larger in size when compared to the prompt splash secondary atomization due to the later stage of the detachment where the crown has a higher thickness. Overall, the droplets originated from prompt splashing present a smaller size when compared to the detached droplets of a fully developed crown rim.

Figure 4.2 exhibits the comparison between the experimental and numerical results at different stages for the crown splash phenomenon for $D_0 = 3.2mm$, $U_0 = 4.1m/s$ and $h^* = 0.27$. The initial frames for $t = 0ms$ are provided as a reference for the different outcomes for further comparison.

Once the droplet impacts onto the liquid film, the crown begins to expand radially and upwards, as can be verified for $t = 1ms$. However, there is a dissimilarity over this frame, since it is possible to visualize a small number of tiny droplets on the numerical solution, which does not match the experimental result. In comparison with prompt splashing, the quantity of secondary droplets ejected in these early stages is residual, however, it still occurs. There are several reasons that might justify the differences between these results, such as the camera not being able to capture these tiny secondary droplets or the numerical approach forcing prompt splashing to occur. This will also be verified for some of the following cases.

The next stage ($t = 3ms$) shows the crown development and the initial crown splashing. It is observable that, in both cases, splashing begins to occur, where the secondary droplets start to exhibit a greater size when in comparison with the prompt splash secondary atomization. Over time, the crown keeps developing and more droplets are ejected from the crown rim, as visualized for $t = 6ms$ and $t = 9ms$, as it reaches its maximum height and diameter. From that moment forward, the crown slowly begins collapsing until it fully disintegrates. This can be verified for $t = 14ms$, $t = 18ms$ and $t = 21ms$. In general, the numerical and experimental results are in good agreement, as the crown exhibits the desired evolution in the early stages of the impact and gradually breaks down with the formation of further secondary droplets at later stages. Despite the prompt splash occurrence, the overall phenomenon developed in a similar way to the experimental results.

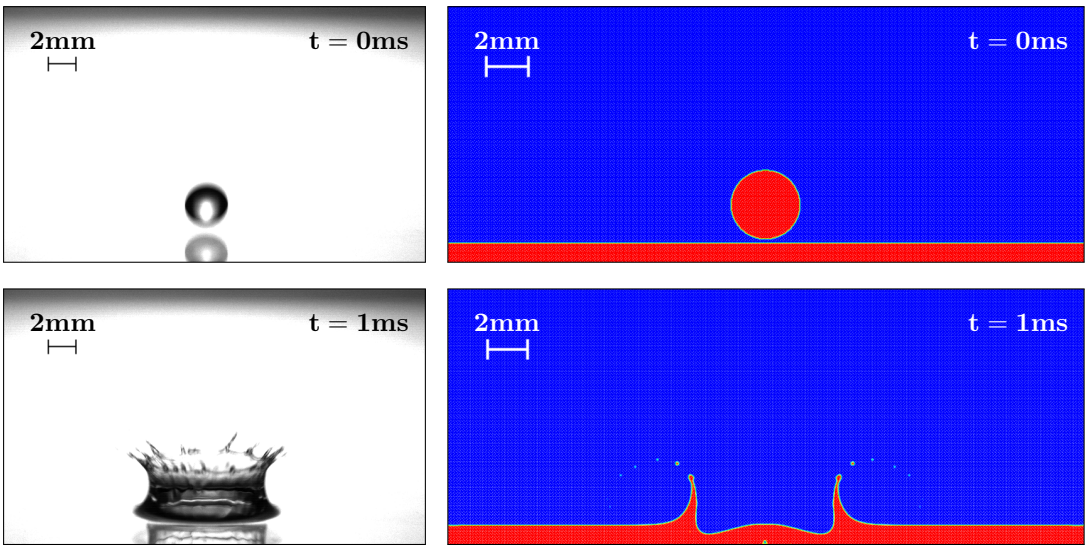

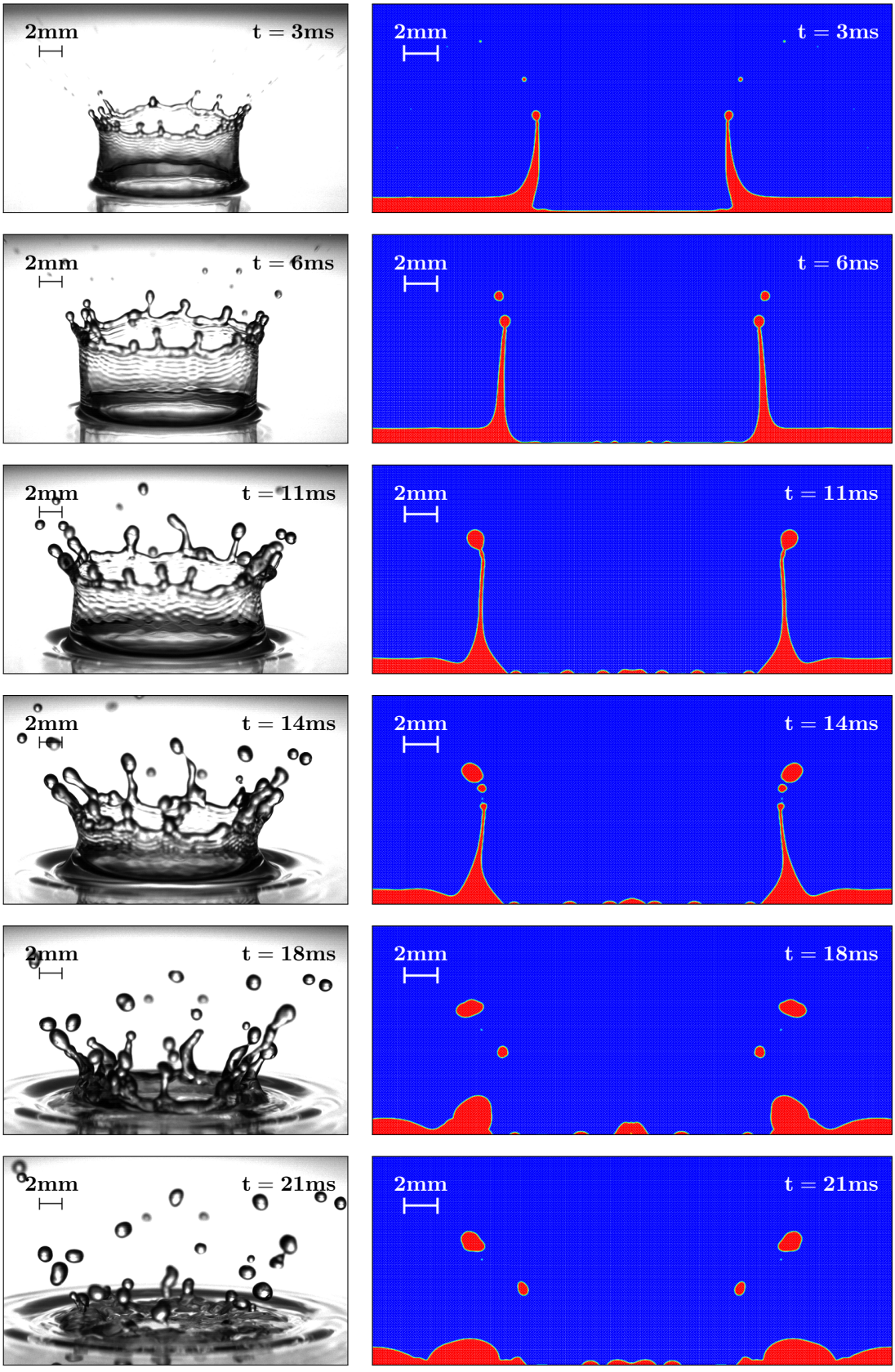

(a) (b)

Figure 4.2: Visualization of the crown splash phenomenon for H_2O ($D_0 = 3.2mm$, $U_0 = 4.1m/s$, $h^* = 0.27$): (a) Experimental Results; (b) Numerical analysis.

4.1.3 Spreading

This phenomenon occurs for low impact velocities where the droplet merges with the liquid film without the formation of secondary droplets. The domain independence study was particularly important for this case, as the capillary waves could influence the impact region if the radial distance was not sufficient. Figure 4.3 illustrates the progression of this phenomenon for $D_0 = 2.8mm$, $U_0 = 1.8m/s$ and $h^* = 1$.

Once the droplet impacts the liquid film ($t = 0ms$), an initial crown is formed ($t = 5ms$). Unlike the previous cases, there is no secondary atomization and the crown hardly develops upwards due to the low-velocity impact. Therefore, this smooth crown will mostly develop in terms of radial distance. Once it reaches a maximum height, the crown tends to weaken, as presented for $t = 15ms$, with an increase in its thickness. From this point forward, the liquid moves inwards to fill the impact region that is now occupied by the gas phase ($t = 30ms$). The liquid maintains its motion towards the impact region and, when it reaches the centre, the motion of the fluid changes for an upward direction, creating a small jet that does not break up, as verified for $t = 40ms$. The last stages of this phenomenon, correspondent to $t = 50, 70$ and $80ms$, relate to the small jet reaching a maximum height, stabilizing onto the liquid film and the several oscillations along the film dissipating. The model predictions are in good agreement with the experimental results for this phenomenon, as verified by the visualization of figures 4.3a and 4.3b.

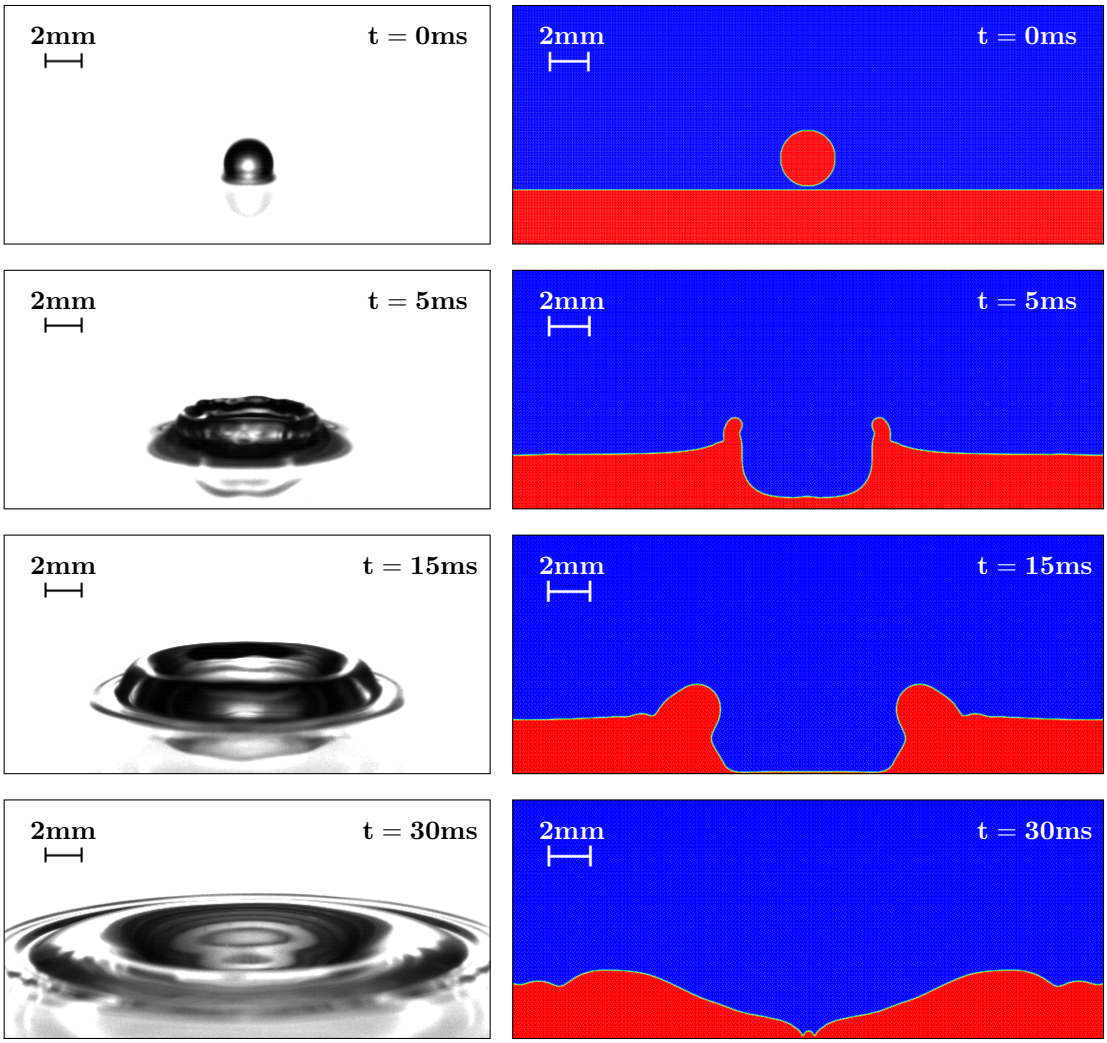

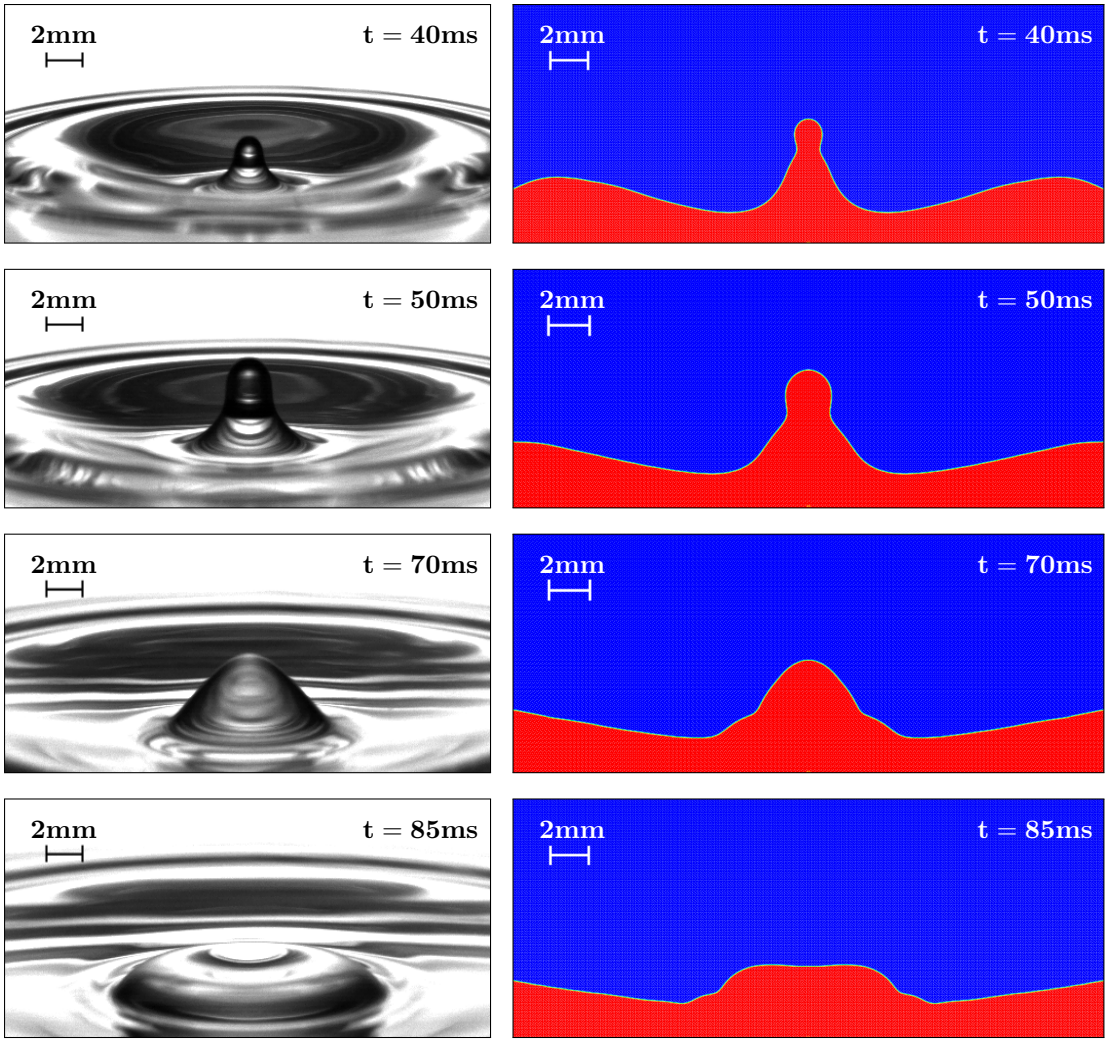

(a) (b)

Figure 4.3: Visualization of the spreading phenomenon for the 75% JF/25% HVO mixture ($D_0 = 2.8mm$, $U_0 = 1.8m/s$, $h^* = 1$): (a) Experimental Results; (b) Numerical analysis.

4.1.4 Jetting

Jetting is a term that several authors adopt to represent different outcomes. Ribeiro [2] defined this phenomenon as a vertical extent of fluid developed after the crown weakening that collapses onto the centre of the impact region and progresses upwards, followed by the ejection of droplets. This definition is selected for this dissertation as well.

Figure 4.4 exhibits the experimental and numerical results of the jetting phenomenon for $D_0 = 3.0mm$, $U_0 = 1.8m/s$ and $h^* = 1$. Initially, the jetting progresses in an equivalent way to spreading. Succeeding the droplet impacting onto the liquid film, for $t = 10ms$, a low height crown rises. When the crown collapses, the fluid proceeds to fill the unoccupied impact region and, when $t = 45ms$, a small jet rises from the centre. This jet continues to grow, both in thickness and height, until a droplet starts detaching from the evolving jet, as can be seen for $t = 60ms$. Once the droplet fully detaches, it will maintain some of its kinetic energy for an upward movement ($t = 65ms$) until gravity forces this droplet onto the liquid film and the phenomenon concludes.

Primarily, it is possible to identify similarities between the experimental and the numerical results. There is no secondary atomization since the droplet detaching from the rising jet is considered a especial case, as mentioned by Ribeiro [2]. The crown development and the droplet formation are also in good agreement with the experimental results.

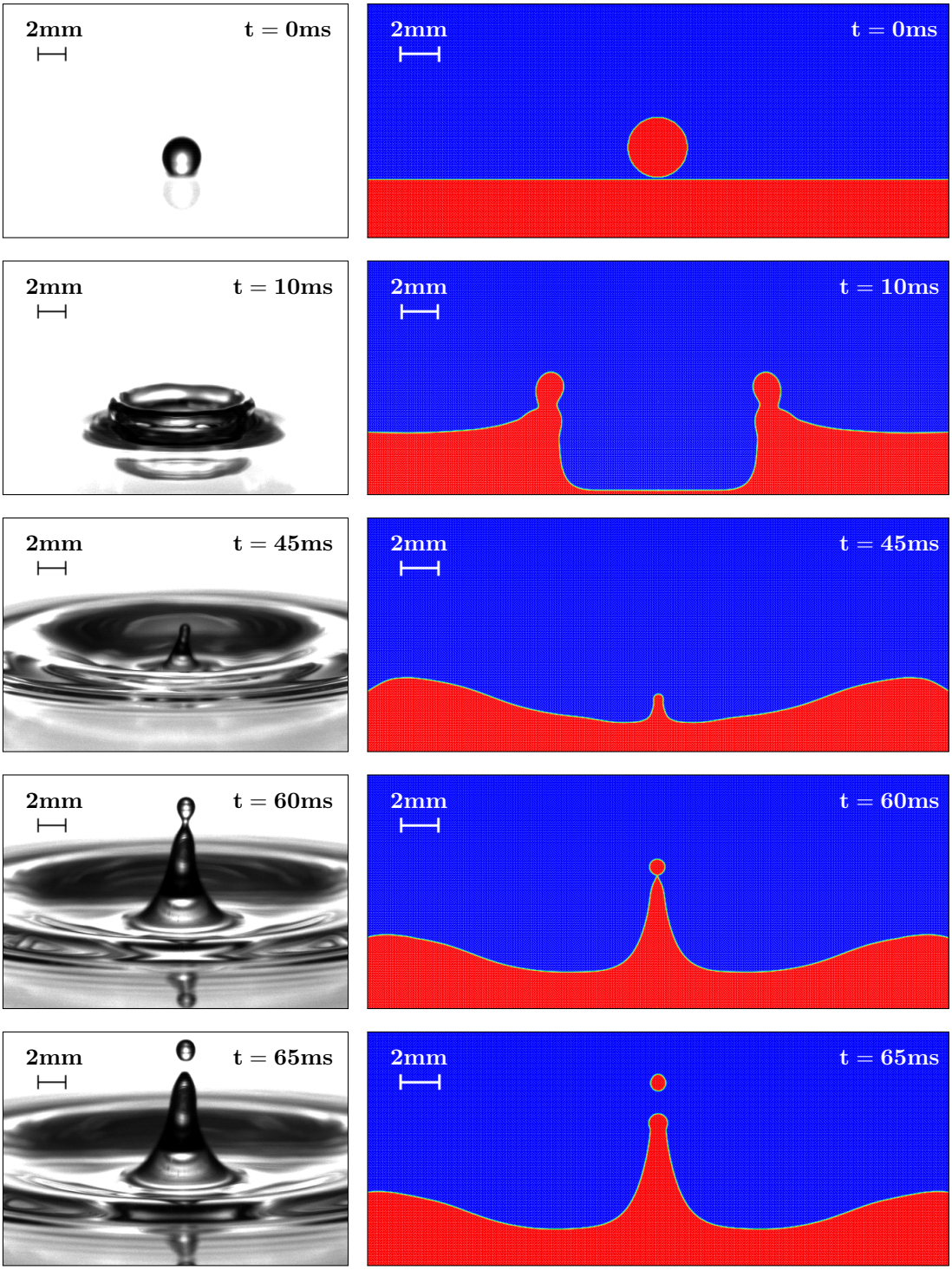

(a) (b)

Figure 4.4: Visualization of the jetting phenomenon for the 100% JF ($D_0 = 3.0mm$, $U_0 = 1.8m/s$, $h^* = 1$): (a) Experimental Results; (b) Numerical analysis.

4.1.5 Fingering

Upon the droplet impacting onto liquid films, and depending on the surface and fluid properties, a thin cylindrical disk, known as the liquid lamella, is formed. Under certain conditions, perturbations on the liquid lamella may grow and extend radially, creating these "fingers". Due to this reason, this phenomenon is denominated as fingering. These fingers may also detach from the lamella, resulting in secondary atomization.

Figure 4.5 exhibits the fingering phenomenon and the respective comparison between the experimental and the numerical results for $D_0 = 2.5mm$, $U_0 = 1.8m/s$ and $h^* = 0.1$. It is noticeable that this outcome displays different characteristics, especially related to the crown rim and development when compared to other phenomena. Following the droplet impact ($t = 2.5ms$), a thin liquid crown rises and rapidly evolves. This crown reaches its maximum height, approximately for $t = 5ms$, and immediately starts decreasing. It is noticeable that, until this point, both the numerical and experimental results are identical in terms of a thin crown being formed and no secondary atomization occurring. However, for $t = 7.5ms$, there are some distinctions between these cases. For the experimental situation, the crown exhibits these disturbances called "fingers". These fingers do not break up into secondary droplets, which does not apply for the numerical simulation. For the numerical results, as it is observable, secondary droplets detach from the crown rim as the crown collapses. From this point forward, the crown breaks down until merging with the pre-existing liquid film ($t = 9ms$ and $t = 9.5ms$), where, for the correspondent experimental frames, fingers around the crown are still fully visible.

This particular case did not present a certain level of accuracy for the numerical results as the previous outcomes. Several ideas arise to justify the results disparity, such as the 2D axisymmetric model not correctly predicting secondary atomization from the liquid lamella or an unreliable modelling approach. Considering the fact that an axisymmetric assumption consists on a model exhibiting symmetry around an axis, and since the droplet impact phenomenon is essentially 3D, axisymmetric crowns emerging subsequent to the droplet impact rarely occur in nature. The fingering phenomenon is an explicit example of this asymmetry, as it is not possible to obtain reliable simulations of these fingers with the current model. Predicting this kind of instabilities imply the need to perform 3D simulations.

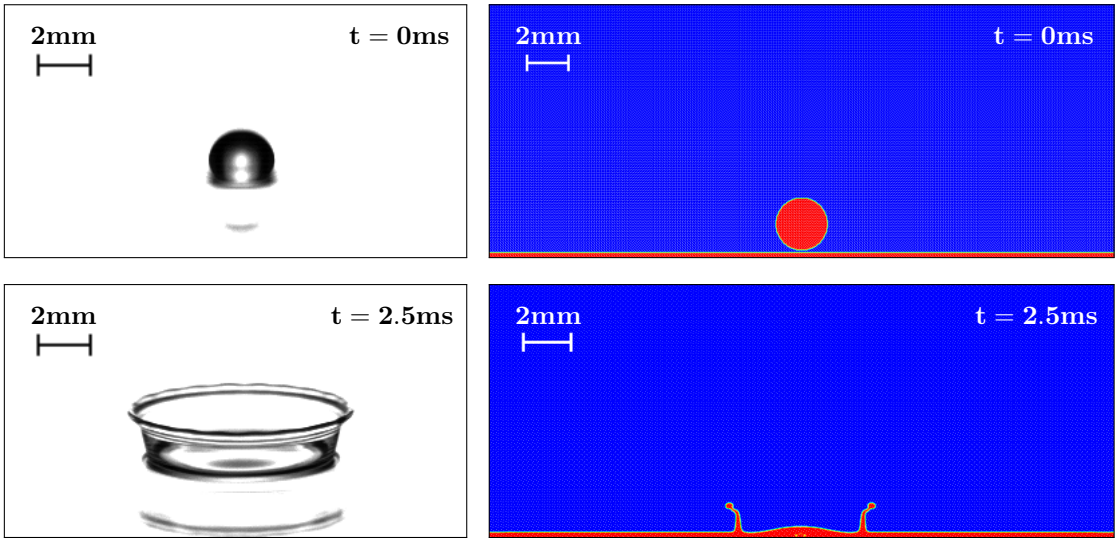

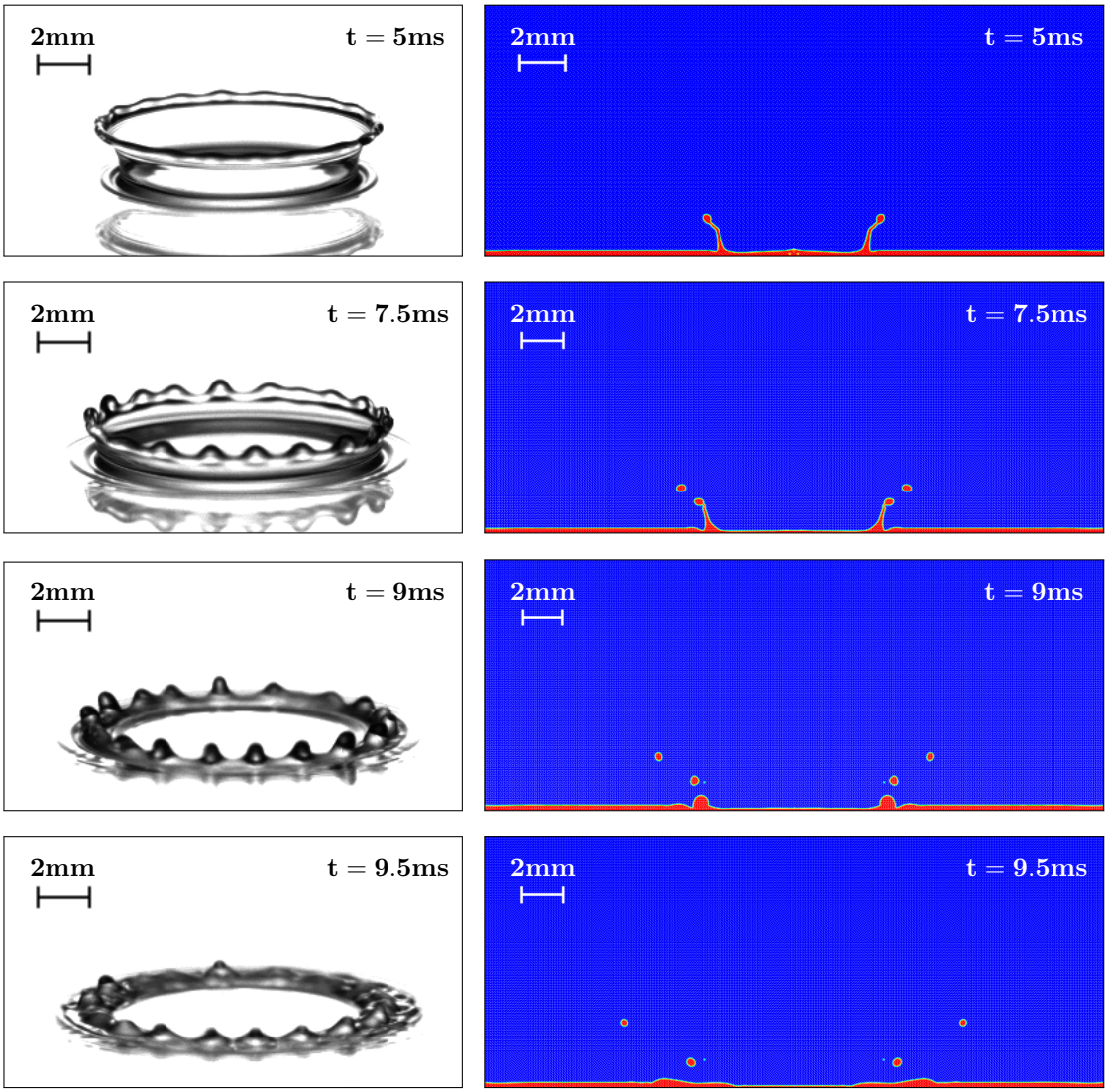

(a) (b)

Figure 4.5: Visualization of the fingering phenomenon for the 75% JF/25% HVO mixture ($D_0 = 2.5mm$, $U_0 = 1.8m/s$, $h^* = 0.1$): (a) Experimental Results; (b) Numerical analysis.

4.1.6 Bubbling

The final outcome reported by Ribeiro [2] is the bubbling. This phenomenon is considered extremely rare, as barely any research is available to comprehend this peculiar event. Upon impact, a high and thin crown is formed up and inwards and, as the crown starts to close, it develops a bubble-like shape. This bubble maintains its form for a certain amount of time until it collapses as a result of external disturbances or energy loss.

Figure 4.6 presents the comparison between the experimental and numerical procedures for the bubbling outcome for $D_0 = 3.1mm$, $U_0 = 4.1m/s$ and $h^* = 0.5$. The first frame represents the moment the droplet impacts onto the liquid film ($t = 0ms$), following the standard approach considered for all of the different outcomes. For $t = 2.5ms$, the initial development of the crown occurs, verifying both prompt and crown splash for the numerical result. However, Ribeiro [2] mentioned that prompt splash did not occur. The reasoning behind this difference was already mentioned over section 4.1.2. Unlike the previous cases, the crown development for

the bubbling is exceptionally distinct, as it reaches a greater height and, as perceivable for $t = 7.5ms$, leans towards the centre. As the outcome progresses, it is possible to recognize a clear divergence between the results. If we visualize the different crowns for $t = 35ms$, the crown is essentially closed for the experimental case, whereas the crown for the numerical simulation is considerably distant from forming a dome and it collapses after a period of time ($t = 42.5ms$), whereas the experimental results show that the crown fully closes and ends up collapsing after a certain period. This development is thoroughly displayed by Ribeiro [2].

The numerical simulation was not able to properly replicate the bubbling phenomenon. Firstly, there is hardly any valuable information in the literature regarding this outcome on how the different physical properties and parameters influence crown growth, splashing, etc. Due to these reasons, numerically reproducing the characteristics that define this peculiar phenomenon is extremely complex, concluding that the current numerical model is not capable of accurately representing bubbling.

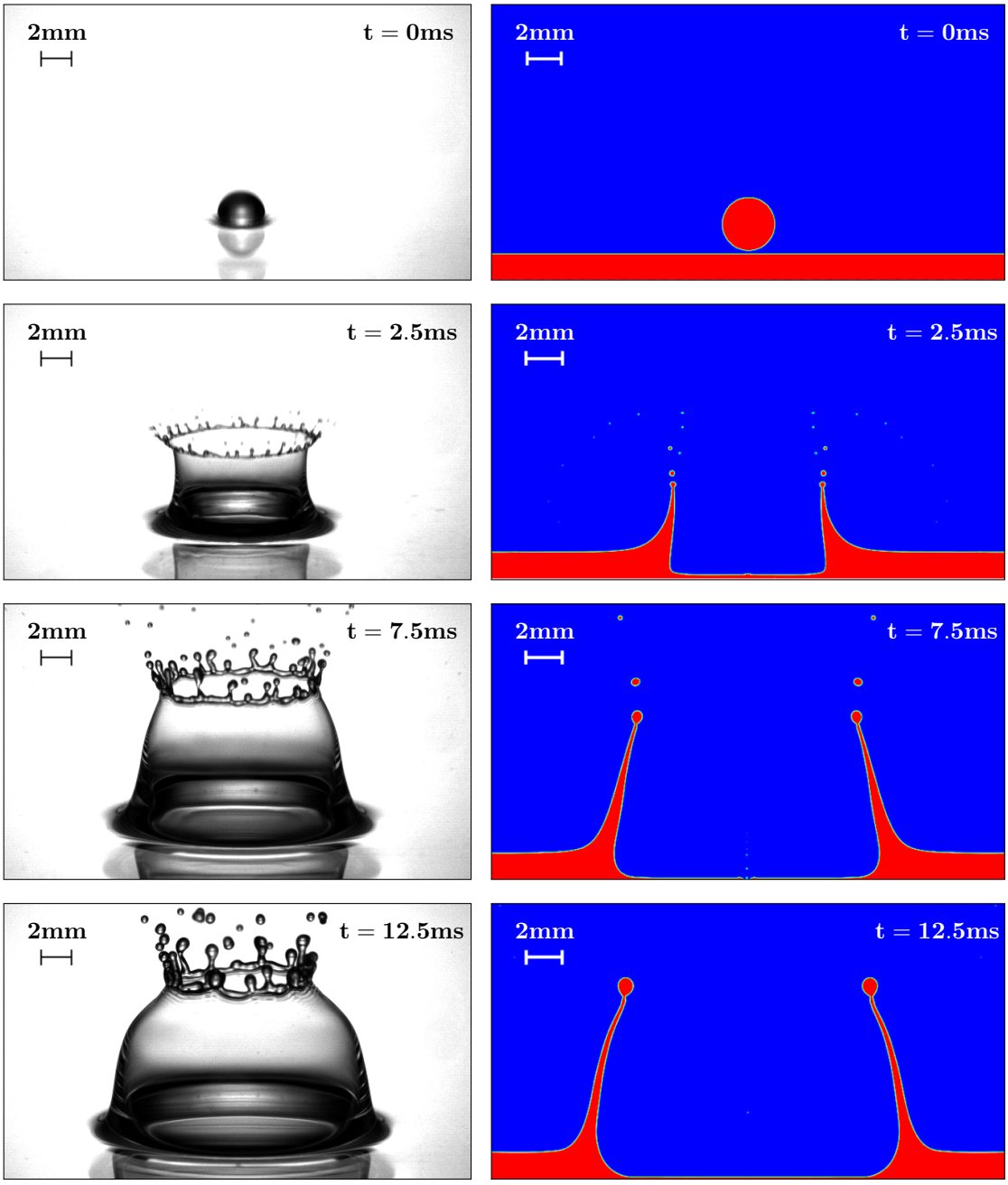

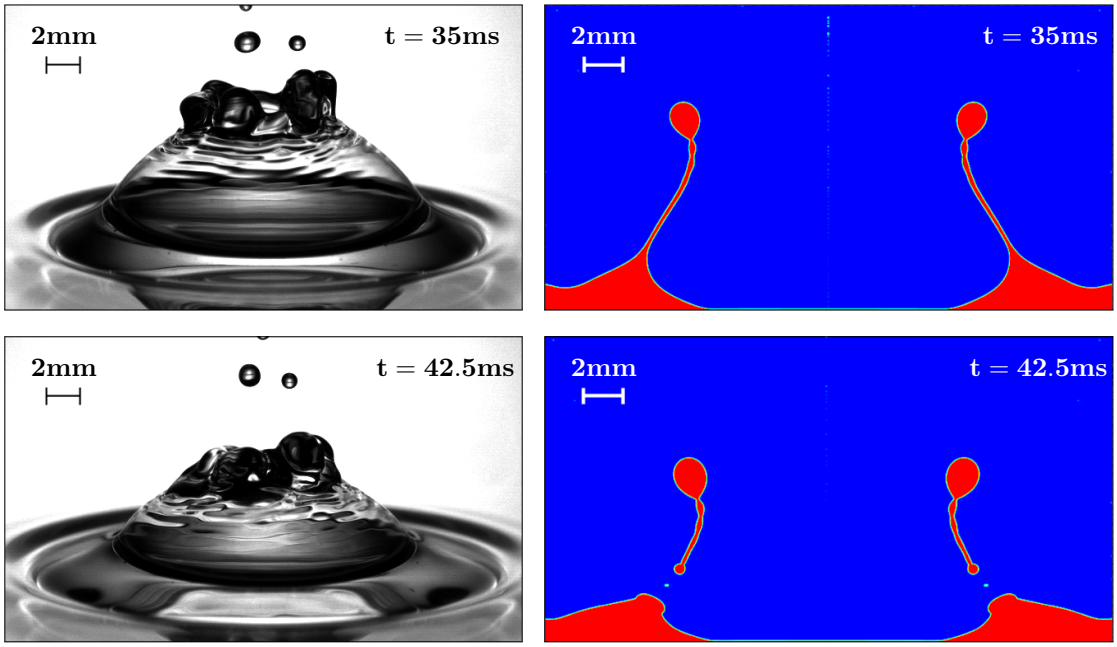

(a) (b)

Figure 4.6: Visualization of the bubbling phenomenon for the 75% JF/25% HVO mixture ($D_0 = 3.1mm$, $U_0 = 4.1m/s$, $h^* = 0.5$): (a) Experimental Results; (b) Numerical analysis.

4.2 Quantitative Analysis

Over section 3.4, the inner diameters of the crown were measured to verify the mesh refinement in the grid independence study. In order to verify if the numerical analysis is comparable to the experimental results, another parameter must be analysed due to difficulties measuring inner diameters of the crown on experimental results. Therefore, the outer diameters of the crown were measured for $t = 2, 4, 6, 8, 12$ and $16ms$, both numerically and experimentally. In terms of the numerical simulations, since the grid size is defined, measuring the outer diameter of the crown is fairly simple, as long as the measurements take place for a particular height of the crown, usually where there is no curvature. Figure 4.7 exhibits the outer diameter of the crown as a function of its height, both non-dimensionalized by the droplet diameter, for $t = 6ms$. It is noticeable that, for a certain range value of H/D_0, the outer diameter barely varies due to the smaller curvature of the crown. Due to this reason, the outer diameter of the crown is measured along that particular zone. It was possible to obtain the several outer diameters of the crown for the experimental results with the support of the MATLAB algorithm analogous to the procedure described in subsection 3.2.1. Figure 4.8 displays the outer diameters of the crown, also non-dimensionalized by the droplet diameter, as a function of the non-dimensional time, for the numerical and experimental analysis.

Lastly, the domain independence study was performed to verify the grid radial distance, $V1$, and the grid height, $H2$. This study is relevant for the computational domain in reducing computational time and CPU expense by not defining over-dimensioned meshes. The dimension that affects the most this kind of impact is the radial distance. Ensuring that the capillary waves formed onto the liquid film subsequent to the droplet impact do not reach the radial wall and rebound into the region where the droplet impact occurs is required to guarantee that the ra-

dial distance does not influence the impact phenomena. Several radial distances were tested, such as $5D_0$, $10D_0$ and $15D_0$. It was verified that, for $10D_0$, the liquid film is not significantly affected at radial distances and, therefore, $V1 = 10D_0$ is adopted for our model. In terms of height, $H2 = 5D_0$ proved to be sufficient to visualize the secondary atomization and the crown development for the different outcomes. These results are consistent with the experimental and numerical studies conducted by Berberović et al. [72].

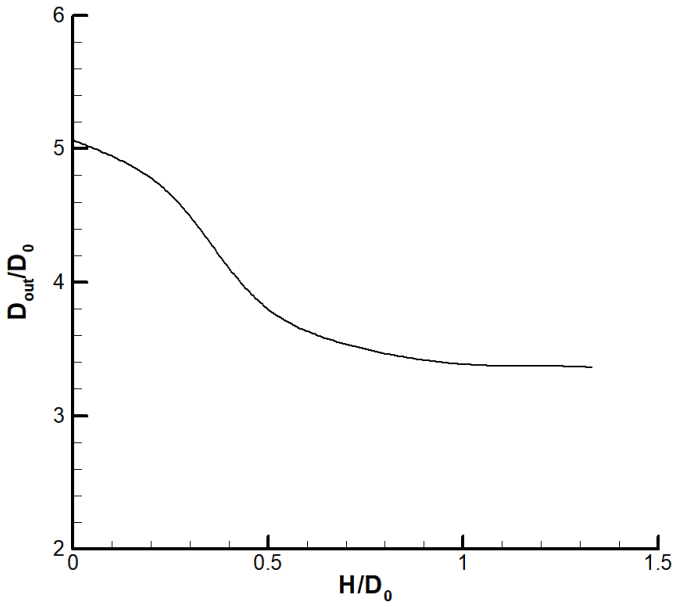

Figure 4.7: Development of the outer diameter of the crown as a function of the crown height, both non-dimensionalized by the droplet diameter, for $t = 6ms$.

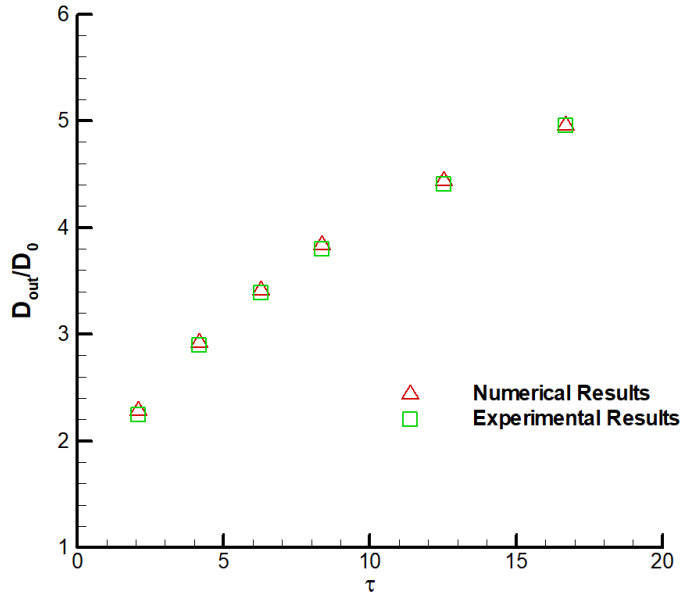

Figure 4.8: Quantitative analysis of the outer diameter of the crown as a function of time, both non-dimensionalized.

4.3 Summary

The current summary recaps the different outcomes and the comparison between the numerical and the experimental results. The validation of the numerical analysis, as the grid height and radial distance, are also presented.

The prompt splash phenomenon exhibits satisfactory crown development and secondary atomisation in the early stages of the impact. The crown splash, despite the overall similarity of the phenomenon in terms of crown progression and collapse, it is visualized prompt splash subsequent to the droplet impact, which does not agree with the experimental results. This may due to the fact that capturing this tiny droplets is rather difficult or that the solution approach for this multiphase flow forces prompt splash onto several situations, as it is also visualized for bubbling. The spreading and the jetting phenomenon are in good agreement with the experimental results. The initial development of a low and thick crown are similar for both circumstances, however, when the liquid phase moves towards the centre region, the jetting phenomenon exhibits a droplet detaching from the evolving jet, while the spreading phenomenon forms a small jet that stabilizes onto the liquid film after a certain duration. The fingering phenomenon displayed several issues regarding finger formation and further break up. In order to correctly predict finger formation and crown development, it is required to perform 3D simulations due to the asymmetry of the droplet impact phenomenon. The final outcome visualized was bubbling. This particular case was not possible to numerically simulate, since the crown collapsed prior to forming the bubble. Understanding the dynamics of bubble formation and crown development for these singular cases is required to subsequently improve numerical simulations.

The outer diameters of the crown were measured for different stages of the phenomenon, as visualized in figure 4.8. This figure is also complemented with figure 4.7, where it is possible to visualize the crown height and its curvature and the region where the measurements occurred.

The grid height and radial distance were $V1 = 10D_0$ and $H2 = 5D_0$, respectively. As visualized on the different outcomes, the different characteristics regarding crown development and secondary atomisation were not affected by the grid radial distance and it was possible to visualize, in terms of height, the secondary droplets and the overall development of the phenomena. This confirms that the grid height and radial distance established were sufficient for the impact to develop.

Chapter 5

Conclusions and Future Work

The final chapter is divided into two different sections. The first relates to the conclusions concerning the reliability of the numerical model in simulating multiphase flows, more specifically the droplet impact dynamics onto liquid films. The differences and similarities of the different outcomes are also explained and correlated to the numerical approach. The second section addresses the following steps that should be taken for future work.

5.1 Conclusions

The vertical impact of a single droplet onto a liquid film was studied numerically to accurately predict liquid-gas interactions and recreate the experimental conditions presented by Ribeiro [2]. The combination of the physical properties of the fluid, droplet diameter, impact velocity and dimensionless thickness provided 180 cases of study, for which only six different outcomes were visualized: prompt splash, crown splash, spreading, jetting, fingering and bubbling. These outcomes were numerically simulated and compared to the experimental data available regarding jet fuel and biofuel mixtures.

The axisymmetric incompressible Navier-Stokes equations are coupled with the VOF multiphase model employing the commercial computational fluid dynamics software ANSYS Fluent 19.0. Gravity, surface tension, viscosity and contact angles for the different fluids are considered for this analysis. The Geo-Reconstruct scheme to track the interface between the phases, the Continuum Surface Force (CSF) model to include the effects of surface tension and the Fractional Step Method (FSM) to solve the incompressible Navier-Stokes equations are used to numerically simulate this phenomenon. The QUICK and PRESTO! schemes are also adopted for momentum and pressure discretization.

The prompt splash phenomenon exhibits secondary atomization in the early stages of the impact drop and the crown evolution appears to be reasonable. Both the spreading and the jetting phenomenon are also in good agreement with the experimental results. The capillary waves formed on the liquid film do not have any influence on the initial impact, proving that the radial distance was sufficient for the current numerical analysis. For the spreading phenomenon, the droplet impacts onto the liquid film, followed by a smooth crown with no secondary atomization. This will develop into forming a small jet that rises upwards and, at later stages, stabilizes onto the liquid film. The jetting phenomenon is relatively similar with the main discrepancy being, as the name suggests, the jet. This jet, unlike the latter phenomenon, continues to grow, both in thickness and height, until a droplet detaches from the rising jet, maintaining its ascending motion and eventually merging with the liquid film due to gravitational forces.

The crown splash phenomenon exhibited a satisfying crown development subsequent to the droplet impact, followed by secondary atomization from the rim at intermediate stages until the crown shatters for later stages of the impact. However, for the earlier stages of the impact,

the numerical analysis showed the occurrence of prompt splash. The quantity of these secondary droplets, when comparing to the prompt splash phenomenon presented in subsection 4.1.1, is significantly lower, but still visible. Ribeiro [2] mentioned that, for the majority of the images, capturing the prompt splash is rather difficult and it is possible that very tiny droplets ejected almost instantly from the ejecta sheet are not visible for the current experimental arrangement. There is also the possibility that the current numerical approach imposes prompt splashing onto particular cases where the impact velocity is relatively higher, as also visualized for the bubbling and, possibly, for the prompt splash phenomenon. Despite not being able to distinguish for the prompt splash, the numerical approach may cause the ejection of more secondary droplets than expected.

The fingering phenomenon presented several issues concerning crown development. The numerical results are in good agreement for the initial droplet impact, followed by an early crown expansion. However, when $t = 7.5ms$, it is observable that the crown rim is not consistent as these structures, called fingers, are formed due to instabilities at the same rim. It is not possible to fully recreate these instabilities of the crown rim numerically due to the initial axisymmetric assumption for the model. Due to these reasons, the numerical results show a reasonable early crown development until crown splashing occurs ($t = 7.5ms$) and, for later stages of the impact, the crown collapses. Predicting this kind of instabilities imply the need to perform 3D simulations for reliable and accurate simulations.

Bubbling is the final visualized outcome. Information regarding the dynamics of this phenomenon is scarce and predicting how the crown develops to form a bubble or dome is an extremely complex subject. Prompt splash is visualized for the earlier stages of the impact in an identical way to the numerical results of the crown splash. The initial crown development is identical for the experimental and numerical results. However, for $t = 35ms$, once the crown starts closing to form a dome, the numerical results show a disparity where the crown is considerably distant from forming a bubble, collapsing after a period of time.

Overall, the results are satisfactory with the experimental observations. Some divergences regarding prompt splashing occurred due to the difficulty in acquiring images where very tiny droplets are ejected or due to the numerical approach imposing the prompt splash phenomenon onto particular cases. The fingering phenomenon displayed inaccurate simulations due to the asymmetry nature of the instabilities, denominated fingers, formed at the crown rim. The bubbling phenomenon requires further research, both experimental and numerically, to better understand the dynamics on bubble formation and progression.

5.2 Future Work

The results in this dissertation provide an initial foundation for numerical analysis regarding the phenomenon of single droplet impact onto liquid films for jet fuel and biofuel mixtures. However, there still are opportunities for further enhancements.

First, 3D analysis should be considered for future work. Despite most of the outcomes being comparable in terms of numerical and experimental results, such as the spreading and the jetting phenomenon, the nature of the phenomenon is three-dimensional due to the fact that regular axisymmetric crowns emerging from the instability of circular lamella rarely occur in nature, implying the need to perform 3D simulations. This was verified for the fingering phenomenon,

where the asymmetry of the crown could not be accurately simulated for the current 2D axisymmetric model. Another advantage of performing 3D simulations is accurately predicting the number, size and velocity of secondary droplets. This study would provide convenient evidence for a more desirable understanding of the dynamics of splashing.

The bubbling phenomenon was one of the outcomes that the numerical approach could not accurately predict. Despite the lack of information for this peculiar event, it is necessary to examine its different stages and investigate, perhaps, a different numerical approach for improved results. Different numerical methods that do not involve the VOF model can also be attempted to represent the droplet impact onto liquid films.

Overall, only six different cases were numerically studied over this dissertation. Following the work developed by Ribeiro [2], there is the possibility of increasing the number of cases, not only in terms of physical properties but also for different surface properties, such as different roughness values or even inclined surfaces.

Bibliography

[1] N. C. on Bioethics, "Biofuels: ethical issues," 2011.

[2] D. Ribeiro, "Experimental study of a single droplet impinging upon liquid films: Jet fuel and biofuel mixtures," Master's thesis, Aerospace Science Department, University of Beira Interior, Covilhã, 2018.

[3] V. Bergeron, D. Bonn, J. Y. Martin, and L. Vovelle, "Controlling droplet deposition with polymer additives," *Nature*, vol. 405, no. 6788, p. 772, 2000.

[4] S. T. Thoroddsen, M. Thoraval, K. Takehara, and T. Etoh, "Droplet splashing by a slingshot mechanism," *Physical review letters*, vol. 106, no. 3, p. 034501, 2011.

[5] A. L. Yarin, "Drop impact dynamics: splashing, spreading, receding, bouncing…," *Annu. Rev. Fluid Mech.*, vol. 38, pp. 159–192, 2006.

[6] C. Motzkus, F. Gensdarmes, and E. Géhin, "Parameter study of microdroplet formation by impact of millimetre-size droplets onto a liquid film," *Journal of Aerosol Science*, vol. 40, no. 8, pp. 680–692, 2009.

[7] G. Liang and I. Mudawar, "Review of mass and momentum interactions during drop impact on a liquid film," *International Journal of Heat and Mass Transfer*, vol. 101, pp. 577–599, 2016.

[8] R. Deegan, P. Brunet, and J. Eggers, "Complexities of splashing," *Nonlinearity*, vol. 21, no. 1, p. C1, 2007.

[9] G. Liang, Y. Guo, and S. Shen, "Gas properties on crown behavior and drop coalescence," *Numerical Heat Transfer, Part B: Fundamentals*, vol. 65, no. 6, pp. 537–553, 2014.

[10] Z. Han, Z. Xu, and N. Trigui, "Spray/wall interaction models for multidimensional engine simulation," *International Journal of Engine Research*, vol. 1, no. 1, pp. 127–146, 2000.

[11] R. Rioboo, C. Tropea, and M. Marengo, "Outcomes from a drop impact on solid surfaces," *Atomization and Sprays*, vol. 11, no. 2, 2001.

[12] A. Moita and A. Moreira, "Drop impacts onto cold and heated rigid surfaces: morphological comparisons, disintegration limits and secondary atomization," *International journal of heat and fluid flow*, vol. 28, no. 4, pp. 735–752, 2007.

[13] C. Bai and A. Gosman, "Development of methodology for spray impingement simulation," *SAE transactions*, pp. 550–568, 1995.

[14] S. S. Yoon and P. E. DesJardin, "Modelling spray impingement using linear stability theories for droplet shattering," *International journal for numerical methods in fluids*, vol. 50, no. 4, pp. 469–489, 2006.

[15] R. F. Allen, "The role of surface tension in splashing," *Journal of colloid and interface science*, vol. 51, no. 2, pp. 350–351, 1975.

[16] H. Marmanis and S. Thoroddsen, "Scaling of the fingering pattern of an impacting drop," *Physics of fluids*, vol. 8, no. 6, pp. 1344–1346, 1996.

[17] S. Thoroddsen and J. Sakakibara, “Evolution of the fingering pattern of an impacting drop,” *Physics of fluids*, vol. 10, no. 6, pp. 1359–1374, 1998.

[18] A. Silva, “Experimental and numerical study of physical aspects of fuel processes,” Ph.D. dissertation, Ph. D. Thesis, Aerospace Science Department, University of Beira Interior, Covilhã, 2007.

[19] G. Coppola, G. Rocco, and L. de Luca, “Insights on the impact of a plane drop on a thin liquid film,” *Physics of Fluids*, vol. 23, no. 2, p. 022105, 2011.

[20] C. Tropea and M. Marengo, “The impact of drops on walls and films,” *Multiphase Science and Technology*, vol. 11, no. 1, 1999.

[21] W. Macklin and G. Metaxas, “Splashing of drops on liquid layers,” *Journal of applied physics*, vol. 47, no. 9, pp. 3963–3970, 1976.

[22] S. Thoroddsen, “The ejecta sheet generated by the impact of a drop,” *Journal of Fluid Mechanics*, vol. 451, pp. 373–381, 2002.

[23] C. Josserand and S. Zaleski, “Droplet splashing on a thin liquid film,” *Physics of fluids*, vol. 15, no. 6, pp. 1650–1657, 2003.

[24] A. Yarin and D. Weiss, “Impact of drops on solid surfaces: self-similar capillary waves, and splashing as a new type of kinematic discontinuity,” *Journal of Fluid Mechanics*, vol. 283, pp. 141–173, 1995.

[25] G. Cossali, M. Marengo, A. Coghe, and S. Zhdanov, “The role of time in single drop splash on thin film,” *Experiments in Fluids*, vol. 36, no. 6, pp. 888–900, 2004.

[26] M. R. Davidson, “Spreading of an inviscid drop impacting on a liquid film,” *Chemical Engineering Science*, vol. 57, no. 17, pp. 3639–3647, 2002.

[27] S. Mukherjee and J. Abraham, “Crown behavior in drop impact on wet walls,” *Physics of fluids*, vol. 19, no. 5, p. 052103, 2007.

[28] A. Coghe, G. Brunello, G. Cossali, M. Marengo, and M.-I. TeMPE-CNR, “Single drop splash on thin film: measurements of crown characteristics,” in *ILASS Europe*, vol. 99, no. 6, 1999.

[29] G. Liang, Y. Guo, S. Shen, and Y. Yang, “Crown behavior and bubble entrainment during a drop impact on a liquid film,” *Theoretical and Computational Fluid Dynamics*, vol. 28, no. 2, pp. 159–170, 2014.

[30] M. Rieber and A. Frohn, “A numerical study on the mechanism of splashing,” *International Journal of Heat and Fluid Flow*, vol. 20, no. 5, pp. 455–461, 1999.

[31] G. Agbaglah and R. Deegan, “Growth and instability of the liquid rim in the crown splash regime,” *Journal of Fluid Mechanics*, vol. 752, pp. 485–496, 2014.

[32] H. Fujimoto, T. Ogino, H. Takuda, and N. Hatta, “Collision of a droplet with a hemispherical static droplet on a solid,” *International journal of multiphase flow*, vol. 27, no. 7, pp. 1227–1245, 2001.

[33] A. I. Fedorchenko and A.-B. Wang, “On some common features of drop impact on liquid surfaces,” *Physics of Fluids*, vol. 16, no. 5, pp. 1349–1365, 2004.

[34] G. Cossali, A. Coghe, and M. Marengo, “The impact of a single drop on a wetted solid surface,” *Experiments in fluids*, vol. 22, no. 6, pp. 463–472, 1997.

[35] C. Motzkus, F. Gensdarmes, and E. Géhin, "Study of the coalescence/splash threshold of droplet impact on liquid films and its relevance in assessing airborne particle release," *Journal of colloid and interface science*, vol. 362, no. 2, pp. 540–552, 2011.

[36] G. Liang, Y. Guo, Y. Yang, N. Zhen, and S. Shen, "Spreading and splashing during a single drop impact on an inclined wetted surface," *Acta Mechanica*, vol. 224, no. 12, pp. 2993–3004, 2013.

[37] C. Motzkus, E. Géhin, and F. Gensdarmes, "Study of airborne particles produced by normal impact of millimetric droplets onto a liquid film," *Experiments in fluids*, vol. 45, no. 5, p. 797, 2008.

[38] R. L. Vander Wal, G. M. Berger, and S. D. Mozes, "Droplets splashing upon films of the same fluid of various depths," *Experiments in fluids*, vol. 40, no. 1, pp. 33–52, 2006.

[39] L. Xu, W. W. Zhang, and S. R. Nagel, "Drop splashing on a dry smooth surface," *Physical review letters*, vol. 94, no. 18, p. 184505, 2005.

[40] L. Xu, L. Barcos, and S. R. Nagel, "Splashing of liquids: Interplay of surface roughness with surrounding gas," *Physical Review E*, vol. 76, no. 6, p. 066311, 2007.

[41] L. Zhang, J. Toole, K. Fezzaa, and R. Deegan, "Splashing from drop impact into a deep pool: multiplicity of jets and the failure of conventional scaling," *Journal of Fluid Mechanics*, vol. 703, pp. 402–413, 2012.

[42] P. Gregory, E. Guthrie, and M. E. Bunce, "Experiments on splash dispersal of fungus spores," *Microbiology*, vol. 20, no. 2, pp. 328–354, 1959.

[43] P. Hobbs and T. Osheroff, "Splashing of drops on shallow liquids," *Science*, vol. 158, no. 3805, pp. 1184–1186, 1967.

[44] F. H. Harlow and J. P. Shannon, "The splash of a liquid drop," *Journal of Applied Physics*, vol. 38, no. 10, pp. 3855–3866, 1967.

[45] F. H. Harlow and J. E. Welch, "Numerical calculation of time-dependent viscous incompressible flow of fluid with free surface," *The physics of fluids*, vol. 8, no. 12, pp. 2182–2189, 1965.

[46] C. W. Hirt and B. D. Nichols, "Volume of fluid (vof) method for the dynamics of free boundaries," *Journal of computational physics*, vol. 39, no. 1, pp. 201–225, 1981.

[47] G. Rocco, G. Coppola, and L. De Luca, "Simulation of drop impact on a thin liquid film by means of the vof method," *Aerotecnica Missili & Spazio*, vol. 89, no. 1, pp. 25–35, 2016.

[48] N. Nikolopoulos, A. Theodorakakos, and G. Bergeles, "Normal impingement of a droplet onto a wall film: a numerical investigation," *International Journal of Heat and Fluid Flow*, vol. 26, no. 1, pp. 119–132, 2005.

[49] M. Sussman, P. Smereka, and S. Osher, "A level set approach for computing solutions to incompressible two-phase flow," *Journal of Computational physics*, vol. 114, no. 1, pp. 146–159, 1994.

[50] M. Sussman and E. G. Puckett, "A coupled level set and volume-of-fluid method for computing 3d and axisymmetric incompressible two-phase flows," *Journal of computational physics*, vol. 162, no. 2, pp. 301–337, 2000.

[51] B. Ray, G. Biswas, A. Sharma, and S. W. Welch, “Clsvof method to study consecutive drop impact on liquid pool,” *International Journal of Numerical Methods for Heat & Fluid Flow*, vol. 23, no. 1, pp. 143–158, 2013.

[52] Y. Guo, L. Wei, G. Liang, and S. Shen, “Simulation of droplet impact on liquid film with clsvof,” *International Communications in Heat and Mass Transfer*, vol. 53, pp. 26–33, 2014.

[53] D. A. Weiss and A. L. Yarin, “Single drop impact onto liquid films: neck distortion, jetting, tiny bubble entrainment, and crown formation,” *Journal of Fluid Mechanics*, vol. 385, pp. 229–254, 1999.

[54] S. Shen, F. Bi, and Y. Guo, “Simulation of droplets impact on curved surfaces with lattice boltzmann method,” *International journal of heat and mass transfer*, vol. 55, no. 23-24, pp. 6938–6943, 2012.

[55] J. Wu, C. Liu, and N. Zhao, “Dynamics of falling droplets impact on a liquid film: Hybrid lattice boltzmann simulation,” *Colloids and Surfaces A: Physicochemical and Engineering Aspects*, vol. 472, pp. 92–100, 2015.

[56] S. F. Kharmiani, M. Passandideh-Fard, and H. Niazmand, “Simulation of a single droplet impact onto a thin liquid film using the lattice boltzmann method,” *Journal of Molecular Liquids*, vol. 222, pp. 1172–1182, 2016.

[57] D. Li, Y. Xu, L. Li, H. Lu, and L. Bai, “Tracking methods for free surface and simulation of a liquid droplet impacting on a solid surface based on sph,” *Journal of Hydrodynamics*, vol. 23, no. 4, pp. 447–456, 2011.

[58] M. Antuono, A. Colagrossi, S. Marrone, and D. Molteni, “Free-surface flows solved by means of sph schemes with numerical diffusive terms,” *Computer Physics Communications*, vol. 181, no. 3, pp. 532–549, 2010.

[59] A. Farrokhpanah, B. Samareh, and J. Mostaghimi, “Droplet impact: A gpu based smoothed particle hydrodynamics (sph) approach,” in *ASME 2012 Fluids Engineering Division Summer Meeting collocated with the ASME 2012 Heat Transfer Summer Conference and the ASME 2012 10th International Conference on Nanochannels, Microchannels, and Minichannels*. American Society of Mechanical Engineers, 2012, pp. 615–623.

[60] J. Xiong, S. Koshizuka, and M. Sakai, “Numerical analysis of droplet impingement using the moving particle semi-implicit method,” *Journal of nuclear science and technology*, vol. 47, no. 3, pp. 314–321, 2010.

[61] H. Xie, S. Koshizuka, and Y. Oka, “Modelling of a single drop impact onto liquid film using particle method,” *International journal for numerical methods in fluids*, vol. 45, no. 9, pp. 1009–1023, 2004.

[62] G. Tryggvason, B. Bunner, A. Esmaeeli, D. Juric, N. Al-Rawahi, W. Tauber, J. Han, S. Nas, and Y.-J. Jan, “A front-tracking method for the computations of multiphase flow,” *Journal of Computational Physics*, vol. 169, no. 2, pp. 708–759, 2001.

[63] D. Izbassarov and M. Muradoglu, “A front-tracking method for direct numerical simulation of viscoelastic interfacial flows.”

[64] M. Muradoglu and S. Tasoglu, "A front-tracking method for computational modeling of impact and spreading of viscous droplets on solid walls," *Computers & Fluids*, vol. 39, no. 4, pp. 615–625, 2010.

[65] A. Fluent, "Release 15.0," *Theory Guide, November*, 2013.

[66] J. Brackbill, D. B. Kothe, and C. Zemach, "A continuum method for modeling surface tension," *Journal of computational physics*, vol. 100, no. 2, pp. 335–354, 1992.

[67] C. M. G. Rodrigues, "Modelling of spray-wall impingement," 2016.

[68] B. Pizziol, "Design and experimental characterization of an air-assisted, impinging-jets atomizer for aeronautical applications with biofuel," 2016.

[69] C. A. Harper and E. M. Petrie, *Plastics materials and processes: a concise encyclopedia*. John Wiley & Sons, 2003.

[70] S. Vafaei and M. Podowski, "Analysis of the relationship between liquid droplet size and contact angle," *Advances in colloid and interface science*, vol. 113, no. 2-3, pp. 133–146, 2005.

[71] J. Hu, X. Xiong, H. Xiao, and K.-t. Wan, "Effects of contact angle on the dynamics of water droplet impingement," in *COMSOL Conference*, 2015.

[72] E. Berberović, N. P. van Hinsberg, S. Jakirlić, I. V. Roisman, and C. Tropea, "Drop impact onto a liquid layer of finite thickness: Dynamics of the cavity evolution," *Physical Review E*, vol. 79, no. 3, p. 036306, 2009.

Appendix A

Papers Accepted to Conference

SUBJECT AREAS: Multiphase Flow (https://www.astfe.org/tfec2019/)

ARTICLE TYPE: Extended Abstract

TITLE: Experimental and Numerical Study of Single Droplets Impinging upon Liquid Films

KEYWORDS: Liquid films, Droplet impinging, Jet A-1, biofuel, Volume of Fluid

AUTHORS: Daniel Vasconcelos[1*], Daniela Ribeiro[1], Jorge M. M. Barata[1], André R. R. Silva[1]

ADDRESS: [1]Aerospace Sciences Department, University of Beira Interior, Rua Marques Avila e Bolama, 6201-001 Covilhã, Portugal

ABSTRACT

The present work addresses the experimental and numerical study of single droplets impinging upon liquid films. This type of study is relevant for quite a few research areas and it has several applications: fuel injection in internal combustion engines, spray painting, cooling, coatings, among others. Jet fuel and biofuel were used since the main goal of this work is the implementation of biofuels in civil aviation in order to reduce the fossil fuel consumption. An experimental facility was designed and built to study the dynamic behavior of the impinging droplet. To enrich the study a wide range of impact conditions was tested. Four different fluids were used: Jet A-1, 75%/25% Jet A-1 and NEXBTL, 50%/50% Jet A-1 and NEXBTL and H_2O. Six different phenomena were spotted: deposition, fingering, prompt splash, crown splash, jetting and bubbling. The same impact conditions were numerically simulated to analyze and visualize the different phenomena. The Navier-Stokes equations are solved by means of the explicit Volume of Fluid (VOF) method for a 2D-axisymmetric assumption. This analysis takes into account gravity, surface tension and contact angles for the different fluids. The Piecewise Linear Interface Calculation (PLIC) scheme to track the interface between the phases, the Continuum Surface Force (CSF) model to include the effects of surface tension and the fractional step method (FSM) to solve the incompressible Navier-Stokes equations are used. The numerical analysis is validated qualitatively by comparison with the experimental results and their main differences allows to understand what still lacks in these simulations.